Research Square

Preprints are preliminary reports that have not undergone peer review.
They should not be considered conclusive, used to inform clinical practice,
or referenced by the media as validated information.

Antibiotic-resistance plasmids encode Evangelion, a widespread mobile antiphage defence system

Rodrigo Ibarra-Chávez

Rodrigo.IbarraChavez@bio.ku.dk

University of Copenhagen https://orcid.org/0000-0002-9056-3055

Aa Haeruman Azam

Japan Institute for Health Security

Kotaro Chihara

Japan Institute for Health Security

Amaru Miranda Djurhuus

University of Copenhagen

Kristine Gottlieb

University of Copenhagen

Azumi Tamura

Japan Institute for Health Security

Thomas Sicheritz-Pontén

University of Copenhagen https://orcid.org/0000-0001-6615-1141

Jonas Madsen

University of Copenhagen https://orcid.org/0000-0003-4830-1796

Kotaro Kiga

Department of Drug Development, National Institute of Infectious Diseases, Japan Institute for Health Security

Article

Keywords:

Posted Date: September 29th, 2026

DOI: https://doi.org/10.21203/rs.3.rs-10859067/v1

License: This work is licensed under a Creative Commons Attribution 4.0 International License.
Read Full License

Additional Declarations: There is **NO** Competing Interest.

Antibiotic-resistance plasmids encode Evangelion, a widespread mobile antiphage defence system

Rodrigo Ibarra-Chavez[1,2]#, Aa Haeruman Azam[*3], Kotaro Chihara[*3], Amaru Miranda Djurhuus*1, Kristine A. Gottlieb[1], Azumi Tamura[3], Thomas Sicheritz-Pontén[2], Jonas S. Madsen[1], Kotaro Kiga[3]

[1] Section of Microbiology, Department of Biology, University of Copenhagen, Copenhagen, Denmark

[2] Centre for Evolutionary Hologenomics, Globe Institute, University of Copenhagen, Copenhagen, Denmark

[3] Department of Drug Development, National Institute of Infectious Diseases, Japan Institute for Health Security, Tokyo, Japan

#corresponding author

***authors contributed equally**

Abstract

Plasmids are major drivers of antibiotic resistance, but whether they also shape bacterial susceptibility to phages remains unexplored. Here, we identify Evangelion, a single-gene anti-phage defence system encoded by a naturally occurring plasmid in methicillin-resistant *Staphylococcus aureus* (MRSA), where it protects against lytic *Silviavirus* phages. Evangelion is frequently associated with antimicrobial-resistance plasmids, many of which carry multiple resistance genes and signatures of horizontal transfer, linking plasmid-associated resistance with bacterial immunity. Evangelion proteins combine a conserved DUF4062/TIR-like core with diversified auxiliary regions, revealing an evolutionarily conserved defence architecture adapted to distinct phage environments. Genetic, structural and evolutionary analyses support a model in which Eva01 responds to intracellular phage replication-associated processes and couples activation of its DUF4062 effector to NAD^+ depletion and abortive infection. Distinct Evangelion lineages protect against different phage groups, suggesting that diversification of their auxiliary regions contributes to adaptation to distinct host-phage environments. Together, our findings define Evangelion as a family of mobile anti-phage systems and reveal that antimicrobial-resistance plasmids can couple antibiotic resistance with anti-phage immunity, potentially shaping bacterial susceptibility to both antibiotics and therapeutic phages.

Introduction

Mobile genetic elements (MGEs) are major drivers of horizontal gene transfer (HGT) and bacterial evolution, mediating the transfer of genes and competing with one another for persistence (Frost et al., 2005; Smillie et al., 2010). Plasmids, prophages, phage satellites, integrative elements and other MGEs can carry functions that benefit their bacterial hosts while also promoting their own maintenance and spread. One important example is anti-phage immunity. Many bacterial defence systems are encoded by MGEs, allowing them to protect host cells from viral predation and to shape the distribution of competing genetic elements, including conflicts between plasmids and other MGEs (Doron et al., 2018; Makarova et al., 2011; Bondy-Denomy et al., 2016; Dedrick et al., 2017; Fillol-Salom et al., 2022; Rousset et al., 2022; Botelho et al., 2023; Pfeifer et al., 2022). However, although the contribution of MGEs to bacterial immunity is increasingly recognised, we know much less about how defence functions intersect with other adaptive traits carried by the same elements, particularly antimicrobial resistance.

Among the diverse repertoire of MGEs, plasmids are especially important because they act as major reservoirs of antimicrobial resistance genes, adapt rapidly to selective pressures and spread across diverse multidrug-resistant bacteria, including the ESKAPE pathogens (Partridge et al., 2018; San Millan, 2018; Ares-Arroyo et al., 2023; GBD Antimicrobial Resistance Collaborators et al., 2024; Cazares et al., 2025). Recent studies have further highlighted plasmids as reservoirs of anti-phage and anti-defence functions, including restriction-modification systems, abortive infection systems, CRISPR-Cas systems and other immune modules (Pinilla-Redondo et al., 2022; Grafakou et al., 2024; Samuel et al., 2024; Zheng et al., 2026). Thus, the outstanding question is not simply whether plasmids can encode anti-phage defence, but whether defence and antimicrobial resistance converge on the same clinically relevant plasmids, allowing individual MGEs to simultaneously influence bacterial responses to antibiotics and phages (Rodríguez-Beltrán et al., 2021; Botelho et al., 2023; Beamud et al., 2024). Such coupling could expose resistance plasmids to an additional selective pressure: phage predation. Defence systems that protect plasmid-bearing hosts during viral attack could favour plasmid persistence independently of antibiotic exposure, while the acquisition of resistance plasmids could in turn alter the phage susceptibility of their bacterial hosts. Yet this connection remains poorly understood experimentally.

Staphylococcus aureus provides a powerful model for studying interactions between MGEs and phages. This pathogen harbours a diverse mobilome composed of plasmids, prophages, pathogenicity islands and defence-associated islands that collectively shape susceptibility to viral infection (Firth et al., 2018; Humphrey et al., 2021). Several anti-phage systems have been characterised in staphylococci, including restriction-modification systems, CRISPR-Cas systems and prophage- or satellite-associated defences (Hossain et al., 2024; Rostøl et al., 2024; Aguayo-González et al., 2026). At the

same time, plasmids are major carriers of antimicrobial-resistance determinants in *S. aureus*, yet whether naturally occurring resistance plasmids themselves alter susceptibility to lytic phages remains poorly understood. This is particularly important in methicillin-resistant *S. aureus* (MRSA), where the genetic determinants that permit survival under antibiotic selection may coexist with functions that determine susceptibility to a second major selective pressure: phage infection (Bernheim and Sorek, 2020; Cui et al., 2025).

This relationship also has potential implications for phage-based antimicrobial strategies. Strictly lytic staphylococcal phages, including *Silviavirus* phages such as ϕMR003 and related viruses, have been investigated as antimicrobial agents against MRSA infections (Peng et al., 2019; Lerdsittikul et al., 2024). However, the success of such approaches depends on the defence landscape of the target strain. Recent work suggests that defence systems can be major determinants of host range in *S. aureus* clinical isolates and that engineered phages can be designed to evade complex MRSA defence repertoires (Voss et al., 2026). If antimicrobial-resistance plasmids carry dedicated anti-phage systems, acquisition of these plasmids could therefore simultaneously confer antibiotic resistance and alter susceptibility to lytic phages. More broadly, co-localisation of resistance and defence functions on the same mobile elements could connect antibiotic selection, phage predation and plasmid persistence in clinically important bacterial populations.

In this Article, using phenotype-guided perturbation of the native mobilome of MRSA strain Mw2, we identify the Evangelion system, a single-gene anti-phage defence system encoded by the antimicrobial-resistance plasmid pMw2. Eva01, the founding member of the family, protects its endogenous *S. aureus* host against lytic *Silviavirus* phages, and related systems are frequently associated with ARG-containing plasmids and occur across diverse bacterial hosts and MGEs. Evangelion proteins combine a conserved DUF4062/TIR-like core with diversified auxiliary regions required for defence, and distinct Evangelion lineages exhibit different phage specificities. Genetic, structural and evolutionary analyses support a model in which Eva01 responds to phage replication-associated processes and couples activation of the DUF4062 core to NAD^+ depletion and abortive infection. Together, our findings reveal that antimicrobial-resistance plasmids can encode mobile anti-viral immunity, linking plasmid ecology and antibiotic resistance to phage susceptibility in clinically relevant pathogens.

Results

pMw2 encodes Eva01, a plasmid-borne defence system against *Silviavirus* phages

To investigate whether resident MGEs contribute to phage susceptibility in *S. aureus*, we systematically removed endogenous MGEs from the MRSA-Mw2 lineage and challenged the resulting strains with a panel of staphylococcal phages. Previous work established

that pMw2 is stably maintained in its native host and imposes little detectable fitness cost under laboratory growth conditions (Dorado-Morales et al., 2021). Loss of the native plasmid pMw2 increased susceptibility to several *Silviavirus* phages, including ϕMR003, ϕeMR003 and ϕ74 (Fig. 1A). Quantification by efficiency of plating confirmed that pMw2 reduced phage propagation by several orders of magnitude, while liquid infection assays showed that pMw2-containing cultures recovered from low-MOI challenge but collapsed at higher phage burdens (Fig. 1A and Fig. S1). Thus, pMw2 confers a conditional anti-phage phenotype consistent with abortive defence.

To identify the responsible locus, we cloned candidate plasmid regions enriched in hypothetical proteins and domains of unknown function (DUF). A single locus encoding a DUF4062-containing protein reproduced the anti-phage phenotype in both Mw2 and RN4220 (Fig. S2). Notably, this gene lies near antimicrobial resistance genes (ARGs) and mobility-associated genes (Fig. 1B), linking anti-phage defence to a clinically relevant plasmid context.

We next defined the minimal functional region, using inducible constructs carrying DUF4062 with different flanking sequences. Constructs encoding DUF4062 retained anti-phage activity following induction by anhydrotetracycline (aTc), and a minimal construct, pEva01v3, conferred robust protection even without induction, consistent with basal activity from local regulatory sequences (Fig. 1C and Fig. S3). The DUF4062 gene encodes a predicted two-part protein consisting of a conserved N-terminal DUF4062 region and a short C-terminal segment lacking recognised domain annotations.

We named this defence system Evangelion**,** inspired by the modular defensive units of Neon Genesis Evangelion. The analogy reflects both the conserved core and specialised auxiliary architecture of the system and its apparent role as an executioner-like defence that sacrifices infected cells to protect the wider bacterial population. Because this gene was sufficient to reproduce the pMw2-mediated anti-phage phenotype, we designated this system Evangelion type 01 (Eva01).

Eva01 displayed a narrow defence spectrum. Strong interference was observed against *Silviavirus* phages, whereas unrelated staphylococcal phages were largely unaffected (Fig. 1D). Liquid infection experiments mirrored these results: Eva01-expressing cultures recovered following low-dose challenge with ϕMR003 or ϕ74, whereas control cultures remained cleared (Fig. 1E). These data identify Eva01 as a *bona fide* plasmid-borne anti-phage system with pronounced specificity towards lytic *Silviavirus* phages.

Eva01 defines a widespread defence lineage frequently found on ARG-containing plasmids

The location of Eva01 on pMw2 raised the possibility that related defence loci are disseminated on clinically relevant plasmids. Comparative analysis revealed Eva01-like genes in diverse plasmid backbones, frequently positioned near ARGs, toxin-antitoxin modules and mobility-associated genes (Fig. 1F and Fig. S4). A closely related Eva01 homologue from *Staphylococcus epidermidis* pQ8 displayed a defence profile similar to *S. aureus* Eva01, whereas more divergent homologues from *Acinetobacter baumannii* and *Lactococcus lactis* did not protect against the staphylococcal phages tested (Fig. 1D, Fig. S5 and Supplementary Table S1).

To define the broader distribution of Eva01-like systems, we screened the plasmid database PLSDB (Molano et al., 2025) using a panel of bacterial Eva01/DUF4062 protein sequences. Non-redundant plasmids containing homologues with at least 40% query coverage per HSP were retained. This identified 447 Evangelion-positive plasmids, of which 327 carried at least one ARG (73.2%; Fig. 2A and Supplementary Table S2). Most were associated with *Staphylococcus* species (202 plasmids, 45.2%) or *Enterococcus* species (159 plasmids, 35.6%). Smaller numbers were identified in *Legionella* (2.9%), *Rhodococcus* (2.5%), *Acinetobacter* and *Synechococcus* (1.1%), Bacillus (0.7%) and Salmonella (0.4%) (Fig. 2B and Supplementary Table S2). Notably, Eva01 homologues were detected in 202 of 3,174 Staphylococcus plasmids represented in PLSDB (6.4%), indicating that Evangelion systems occur in a substantial subset of staphylococcal plasmids.

We next examined transfer-associated features. More than half of Eva01-positive plasmids were classified as mobilisable (55.7%), 98 as conjugative (21.9%) and 24 as oriT-only but lacking an identifiable relaxase or mating-pair formation system (5.4%) (Fig. 2C). Only 76 plasmids (17%) did not have transfer signatures. Among the 376 plasmids encoding an identifiable relaxase, MOBV was the most frequent relaxase family, followed by MOBP and MOBC. These plasmids also carried diverse ARG combinations, most commonly β-lactamase, aminoglycoside, cadmium and macrolide resistance determinants (Fig. 2D and Supplementary Table S2). Most ranged from 10-100 kb and carried a median of five ARG annotations (Fig. 2E). Representative MOB-suite classifications for the curated loci are summarised in Supplementary Table S1.

Therefore, Eva01 is not an isolated feature of staphylococcal plasmids but defines a widespread plasmid-associated defence lineage frequently found on ARG-rich and transferable plasmids.

Evangelion systems encode a conserved DUF4062/TIR-like effector core

To define the molecular architecture of Evangelion proteins, we next examined Eva01 within the context of this widespread plasmid-associated defence lineage. Conserved domain analysis (Wang J et al, 2023) and AlphaFold3 (Abramson et. al, 2024) predicted that Eva01 contains a compact N-terminal DUF4062 region with an α/β fold resembling

TIR-like proteins, followed by a short C-terminal auxiliary region (AUX) (Fig. 3A). A putative ADP/NAD^+-binding pocket was identified within the DUF4062/predicted TIR-like core, suggesting that this region may contribute to nucleotide processing.

Although DUF4062-containing proteins have been identified in diverse bacterial genomes, their biological function remains poorly understood (Wang et al., 2023). To place Evangelion proteins in an evolutionary context, we compared representative Eva/DUF4062 cores with bacterial and eukaryotic TIR domains and TIR-like proteins, including ThsB-family sensors and nucleotide-associated defence proteins (Essuman et al., 2017; Horsefield et al., 2019; Wan et al., 2019; Ofir et al., 2021; Leavitt et al., 2022; Ka et al., 2020; Roberts et al., 2025). Maximum-likelihood phylogenetic analysis resolved Evangelion proteins as a distinct DUF4062-associated lineage that was clearly separated from canonical bacterial TIR proteins and ThsB-family sensors (Fig. 3B and Supplementary Table S5). These results suggest that Evangelion proteins belong to a broader group of TIR-like nucleotide-associated proteins (Wang et al., 2023; Osinski et al., 2026).

To examine conservation within the family, we aligned representative Evangelion proteins spanning diverse bacterial hosts and MGE contexts. Despite extensive divergence within the AUX region, the DUF4062 core contained several highly conserved motifs (Fig. 3C and Fig. S6). These included an N-terminal aromatic motif centred on phenylalanine F11, a conserved acidic-SYT region containing a putative catalytic glutamate E87, and a DUF4062-specific region encompassing glutamine-tryptophan-glutamic acid Q/W/E. Conservation of these residues across phylogenetically distant Evangelion proteins suggested that they contribute to a shared biochemical function.

Using AlphaFold3 modelling and structural superposition with representative TIR and TIR-like proteins, we found a conserved fold of the DUF4062 core despite limited primary-sequence similarity (Fig. 3D). Mapping conserved residues onto the predicted model positioned F11 and E87-Y88 within a common surface pocket of the DUF4062 core, consistent with a potential catalytic or ligand-binding role.

The DUF4062 core and AUX region function cooperatively during Evangelion defence

The predicted DUF4062 pocket and the conservation of F11, E87 and W162 suggested that the core region of Eva01 may provide the biochemical output of the system. To test this, we generated an evolution-guided panel of Eva01 variants targeting the DUF4062 core, the DUF4062-AUX junction and the AUX region (Fig. 4A-B and Fig. S5). Because lysine/arginine-density analysis revealed positively charged patches near the DUF4062-AUX interface and within AUX, we also included mutations designed to probe regions with potential nucleic-acid-interaction properties (Fig. 4B).

Spot assays and phage-yield measurements showed that F11A, E87A, W162A, W162F and the AUX truncation Eva01::L177* disrupted defence against *Silviavirus* phages, producing susceptibility and phage titres comparable to inactive controls (Fig. 4C,D). W162F retained only weak residual activity in liquid infection assays, indicating that aromatic substitution is insufficient to replace the native tryptophan at this position (Fig 4E). By contrast, Eva01::F212A retained protection against ϕ74 but showed impaired defence against ϕMR003, suggesting that individual AUX residues can differentially affect responses to distinct *Silviavirus* phages.

Because structural analyses identified a putative nucleotide-associated pocket within DUF4062, we next examined the metabolic consequences of Evangelion activation during phage infection. Untargeted polar LC-MS analysis performed 15 minutes after ϕMR003 challenge revealed pronounced alterations in adenine-associated metabolites in cells expressing wild-type Eva01 relative to inactive mutants (Fig. 4F). Compared with E87A and L177*, wild-type Eva01 displayed reduced NAD^+ abundance together with broader perturbations in adenine-containing metabolites, including guanosine, adenosine, adenine and related nucleotide derivatives. Although these measurements do not directly establish enzymatic activity, they indicate that Evangelion activation is associated with nucleotide-metabolic remodelling during infection (Fig. 4F and Fig. S7).

To investigate how the DUF4062 core and AUX region might communicate, we modelled Eva01 using AlphaFold3. The resulting structure positioned the DUF4062 domain and AUX region in close physical proximity despite their distinct folds, with W162 near the predicted dimer interface and F212 within a conserved AUX pocket (Fig. 4G-J). Modelling of the N-terminal DUF4062-containing region further predicted dimeric assemblies with stacked interfaces in both NAD^+- and ADP-bound models (Fig. S8A-B). Consistent with this, recombinant Eva01 purified from *E. coli* resolved by mass photometry as multiple species, including masses compatible with dimeric and higher-order assemblies (Fig. S8D). These observations suggest that Eva01 can self-associate, although the role of oligomerisation in defence activation remains to be determined.

Phage escapers implicate replication proteins in Evangelion activation

To identify candidate determinants of Evangelion susceptibility, we isolated spontaneous escaper mutants of ϕMR003 and ϕ74 capable of infecting Eva01-containing cells (Fig. 5A and S9A-B). Whole-genome sequencing revealed that independent ϕMR003 escapers repeatedly acquired mutations in a region encoding a RecA/Sak-like recombination protein and a neighbouring homing-endonuclease-remnant gene (HEG) (Fig. 5B and Supplementary Table S6). Similarly, ϕ74 escapers accumulated mutations within a UvsX-like recombination protein and an adjacent hypothetical gene (Fig. 5C).

To determine whether these loci were shared among Eva01-sensitive phages, we compared the corresponding genomic regions across multiple *Silviavirus* genomes. Comparative analysis showed that these loci reside within a conserved module enriched in recombination- and replication-associated genes, including RecA/Sak-like and UvsX-like homologues (Fig. 5D and S9C). The convergence of escaper mutations on this shared module suggested that Eva01 activation is associated with conserved replication functions rather than highly variable structural components of the virion.

Eva01 restricts intracellular phage genome accumulation after DNA entry

Because escaper mutations repeatedly targeted phage recombination-associated proteins, we asked whether Eva01 preferentially interacts with DNA structures resembling replication or recombination intermediates. Purified Eva01 was incubated with a panel of DNA substrates representing blunt double-stranded DNA (dsDNA), single-stranded DNA (ssDNA), 3' overhang DNA, gapped DNA and bubble DNA. Eva01 exhibited the strongest mobility shift with the 3' overhang substrate, whereas little or no binding was observed for blunt dsDNA or ssDNA. Intermediate binding was detected for gapped DNA, while only weak binding was observed for bubble DNA (Fig. 5E). This substrate preference is further supported by concentration-dependent binding of Eva01 to the 3' overhang substrate (Fig. S8C), consistent with the genetic evidence implicating replication-associated phage functions in Evangelion susceptibility.

We next tested whether Eva01 affects phage genome accumulation during infection. Cultures carrying Eva01 or an empty-vector control were challenged with wild-type ϕMR003, whereas Eva01-containing cells were additionally infected with the escaper mutant ϕMR003 E10. Intracellular phage DNA abundance was quantified by digital PCR using primers targeting two independent genomic loci and normalised to the *S. aureus* reference gene *gyr*B. Digital PCR targeting the capsid and *uvs*X genes showed that both phage markers remained detectable following infection, demonstrating that phage DNA enters Eva01-containing cells (Fig. 5F). However, accumulation of both loci was markedly reduced relative to the empty-vector control, indicating that Eva01 acts after DNA injection and restricts productive phage genome amplification. Early increases in phage

DNA abundance further suggest that replication is initiated but does not proceed efficiently in the presence of Eva01.

In contrast, ϕMR003 E10 restored intracellular phage DNA accumulation despite the presence of Eva01 (Fig. 5F). Similar trends were observed for both capsid and *uvs*X, indicating that the effect was not restricted to a specific region of the phage genome. Thus, escape mutations that enable plaque formation in Eva01-containing cells also restore phage genome accumulation during infection.

Although the precise activating signal remains unknown, the repeated selection of mutations within homologous recombination-associated loci across independent escapers and distinct *Silviavirus* phages points to a common underlying mechanism. The convergence of mutations in UvsX-like and RecA/Sak-like functions, together with the observation that phage genomes are detectable in Eva01-containing cells but fail to accumulate efficiently thereafter, suggests that Evangelion defence is linked to conserved replication-associated processes. Whether Eva01 directly senses phage recombination proteins or instead responds to replication intermediates generated during infection remains an important question for future investigation.

DUF4062-containing proteins form evolutionarily distinct defence-associated lineages

Having established Eva01 as the founding member of the Evangelion defence family, we next investigated the evolutionary diversity of DUF4062-containing proteins in bacteria. We analysed approximately 6,000 bacterial proteins containing the DUF4062 domain (PF13271) and used this dataset to examine the distribution of DUF4062-containing proteins across bacterial genomes and MGEs. Phylogenetic analysis resolved several distinct DUF4062-associated lineages recovered from plasmids, prophages, phage satellites, integrative elements and chromosomal loci (Fig. 6A-B and S10A). Among these, Eva01 formed a well-supported clade containing homologues from diverse staphylococcal and other MGEs, while additional clades contained the representative systems Eva02-Eva04. Together, we designate these experimentally and genomically characterised DUF4062-AUX defence lineages as the Evangelion family. The recently described Swarożyc system and bacterial TEP1-like proteins occupied distinct branches within the broader DUF4062 phylogeny and were therefore retained as related, but separate, groups.

Despite substantial sequence divergence, representative proteins retained several conserved DUF4062 motifs, including the putative catalytic E-Y region and the characteristic Q/W/E motif (Fig. 6C). Structural modelling further supported a common evolutionary origin. AlphaFold predictions of representative Evangelion proteins from *S. aureus*, *A. baumannii*, *Escherichia coli*, *Enterococcus faecalis* and the Swarożyc

system of *Klebsiella pneumoniae* revealed a conserved DUF4062 core architecture despite extensive divergence elsewhere in the protein (Fig. 6D and S10B). In contrast, the auxiliary regions varied markedly in length, topology and predicted surface properties. Consistent with this broader relationship, Conserved-domain searches identified DUF4062 as the shared feature between Eva01 and bacterial TEP1-like proteins, whereas TEP1-like homologues contained additional TROVE, NACHT and WD40-repeat domains, consistent with distinct biological contexts (Fig. S11). The presence of these domains strongly supports an evolutionary link to eukaryotic TEP-1 proteins of the RNA vault.

These observations indicate that Evangelion proteins belong to a broader and evolutionarily diverse superfamily of DUF4062-containing proteins that share a conserved structural core.

Distinct Evangelion lineages exhibit specialised defence profiles

The conservation of the DUF4062 core together with extensive diversification of auxiliary regions suggested that distinct Evangelion lineages may have evolved specialised defence activities. To test this possibility, representative systems from different lineages were challenged with phage panels in their respective experimental hosts.

Interestingly, Eva01 preferentially restricted staphylococcal *Silviavirus* phages, including ϕMR003 and ϕ74 (Fig. 6E and Supplementary Table S1). By contrast, Eva03 displayed a distinct defence profile and interfered with members of the BASEL phage collection belonging to the *Dhillonvirus* genus (Maffei et al., 2021). Although the magnitude of protection conferred by Eva03 was lower than that observed for Eva01, these experiments demonstrate anti-phage activity in a phylogenetically distant bacterial host. In contrast, Eva02 did not confer detectable protection against the phages tested in either *S. aureus* or *E. coli* under the conditions examined.

Collectively, these findings define Evangelion as a broader family of DUF4062-based defence systems that has diversified across bacterial hosts and MGEs while retaining a conserved structural core. The distinct defence spectra of Eva01 and Eva03 further indicate that diversification of Evangelion proteins is accompanied by diversification of anti-phage activity. Thus, conservation of the DUF4062 core is compatible with extensive functional diversification, allowing distinct Evangelion lineages to adapt to different host-phage environments.

DUF4062 and AUX regions function as co-evolved defence modules

The conservation of DUF4062 across Evangelion lineages and bacterial TEP1-like proteins raised the question of whether this domain retains functional features across distant biological contexts. Structural comparison of Eva01 and human TEP1 revealed

similarity between their DUF4062 regions, including a predicted nucleotide-binding pocket within the shared core fold (Fig. 7A and S12). In TEP1, DUF4062 is embedded within a large multidomain protein, whereas in Eva01 it is coupled to a compact AUX region that is required for anti-phage defence (Fig. 7B). To test whether the eukaryotic DUF4062 domain could function within an Evangelion protein, we generated chimeras in which segments of the Eva01 DUF4062 region were progressively replaced with the corresponding region from human TEP1 while retaining the Eva01 AUX domain (Fig. 7C).

Complete replacement of the Eva01 DUF4062 region with the corresponding TEP1 segment failed to restore defence (Fig. 7D-E). However, several intermediate chimeras retained weak but reproducible activity against ϕMR003 and ϕ74, most notably Eva01::HsTEP1-E. Although substantially weaker than wild-type Eva01, these constructs consistently reduced phage susceptibility relative to inactive controls, indicating partial functional compatibility between bacterial and eukaryotic DUF4062 domains.

Structural modelling of the chimeric proteins showed that active and inactive chimeras retained similar overall architectures, arguing against gross misfolding as the sole explanation for loss of defence (Fig. 7F). Instead, the strongest residual activity was observed in constructs preserving regions surrounding conserved Eva01 residues and the predicted DUF4062-AUX interface. This pattern suggests that defence requires local compatibility between the DUF4062 core and the Eva01 AUX region.

The partial activity of TEP1-derived chimeras is notable given recent work showing that human TEP1 functions as a DUF4062-dependent NADase within vault ribonucleoprotein particles (Osinski et al., 2026). These results suggest that DUF4062 domains retain conserved biochemical features across distant biological contexts, but that robust anti-phage defence requires a co-adapted DUF4062-AUX unit.

Discussion

Our findings reveal that a clinically relevant antimicrobial-resistance plasmid can directly alter phage susceptibility by encoding a dedicated anti-phage defence system. Evangelion was discovered on the MRSA plasmid pMw2, where it protects against lytic *Silviavirus* phages and forms part of a broader family of mobile defence systems distributed across diverse bacterial hosts and MGEs. Thus, pMw2 illustrates how clinically relevant plasmids are not merely vehicles for antimicrobial resistance, but also important reservoirs of anti-phage immunity. These observations are consistent with recent studies identifying diverse defence systems on plasmids (Grafakou et al., 2024; Zheng et al., 2026) and support the emerging view that MGEs contribute substantially to the bacterial pan-immune system (Bernheim and Sorek, 2020).

The frequent association of Eva01-like systems with ARG-rich plasmids suggests that phage defence may be one of the accessory traits that shapes the success of resistance plasmids. Plasmid persistence is usually considered through the balance between mobility, fitness cost, antibiotic selection and host range (Frost et al., 2005; Smillie et al., 2010; San Millan, 2018; Partridge et al., 2018). Our study adds phage predation to this framework. By protecting host populations during viral attack, plasmid-encoded defence systems could provide episodic but strong selective benefits that favour maintenance of ARG-containing plasmids even outside antibiotic exposure. More broadly, recent work has shown that plasmid evolution is shaped by population-level interactions among MGEs, antibiotics and phages, with ecological selection determining which plasmid architectures are maintained over time (Rodríguez-Beltrán et al., 2021; Sastre-Dominguez et al., 2026; Ipoutcha et al., 2026). In addition, conjugative plasmids encode anti-defence systems that promote establishment during HGT, further illustrating how plasmid cargo can overcome immunity and shape dissemination (Samuel et al., 2024). In this context, phage defence systems such as Evangelion may provide an additional selective advantage that promotes the maintenance and dissemination of resistance plasmids even in the absence of direct antibiotic selection. Conversely, the same defence cargo could influence plasmid ecology by altering phage-mediated transfer, host survival and competition among co-resident MGEs.

In *S. aureus*, plasmids, prophages, pathogenicity islands and defence-related islands collectively shape genome evolution and phage susceptibility (Humphrey et al., 2021; Hossain et al., 2024; Kuang et al., 2026; Voss et al., 2026). Our study suggests that resistance plasmids can also encode potent anti-phage systems. Consequently, the MGE content of a strain may represent an underappreciated determinant of therapeutic phage efficacy, particularly for MRSA and other ESKAPE pathogens.

Our data identify DUF4062 as the conserved core of Evangelion systems. DUF4062-containing proteins are widespread but remain poorly characterised, and our structural analyses place Evangelion proteins within a divergent TIR-like family. This finding is

consistent with the growing appreciation that TIR-domain and TIR-like proteins function as nucleotide-processing effectors in bacterial immunity (Ofir et al., 2021; Wang et al., 2024). In Eva01, conserved DUF4062 residues were required for defence, and phage infection was associated with pronounced alterations in NAD^+-linked and adenine-associated metabolites. Although these observations do not establish the biochemical activity of Eva01 directly, they support a connection between Evangelion activation and nucleotide metabolism.

Notably, TIR-like domains are not universally associated with antiviral defence. The *S. aureus* TIR-domain protein TirS acts as a virulence factor that suppresses host Toll-like receptor signalling and promotes bacterial persistence during infection rather than mediating bacterial immunity (Askarian et al., 2014). More broadly, TIR and TIR-like proteins have diversified extensively across bacteria, plants and animals, where they participate in functions ranging from immune signalling to host-pathogen interactions and stress responses (Lapin et al., 2022; Yirmiya et al., 2025). The evolutionary relationship between Evangelion proteins and TEP1-like DUF4062 proteins therefore raises the possibility that DUF4062 proteins have undergone similar functional diversification while the domain itself has retained conserved biochemical properties.

The recent demonstration that a DUF4062-containing protein can function as TIR-like NADases provides a useful framework for interpreting these results. In particular, Osinski and colleagues reported that human TEP1 functions as an NADase within vault ribonucleoprotein particles (Osinski et al., 2026). Although the biological contexts differ substantially, the partial functionality of TEP1-derived chimeras in the Eva01 background suggests that bacterial Evangelion systems and eukaryotic TEP1-like proteins retain features of a common biochemical scaffold. Whether DUF4062 proteins share a conserved catalytic mechanism remains unresolved.

Our mutational and chimera analyses further demonstrate that Evangelion activity depends on cooperation between the conserved DUF4062 core and the variable AUX region. AUX truncation abolished defence, mutations at the DUF4062-AUX interface impaired activity, and replacement of Eva01 DUF4062 segments with human TEP1 sequences restored only partial protection despite preserving overall protein architecture. These observations support a model in which DUF4062 and AUX regions function as co-evolved modules rather than independently interchangeable parts. Similar architectures are common among bacterial immune systems, where conserved effector domains are coupled to variable sensing or regulatory modules that determine activation specificity (Doron et al., 2018; Payne et al., 2021; Rousset et al., 2022).

The escaper and dPCR experiments place Evangelion activity after phage DNA entry. Independent escaper mutants repeatedly acquired mutations within a conserved genomic region associated with HEG-related functions and neighbouring RecA/Sak-like and UvsX-like proteins involved in phage recombination and replication. These mutations

arose independently in two distinct *Silviavirus* phages and converged on a shared replication-associated module, suggesting that Eva01 activation is connected to conserved intracellular processes rather than phage-specific structural components. Consistent with this model, Eva01 preferentially associated with recombination-like DNA substrates and reduced intracellular phage genome accumulation without preventing DNA entry. Together, these observations place Evangelion among defence systems that act after genome injection and suggest that activation occurs during early stages of phage genome processing. Whether Eva01 responds directly to phage recombination proteins, recognises replication-associated DNA structures, senses HEG-associated activities or detects downstream metabolic perturbations remains unresolved. The repeated recovery of escaper mutations within a conserved HEG-associated module, together with recent evidence that homing endonucleases can promote anti-defence functions during infection (Chihara et al., 2026), identifies this region as a promising target for future mechanistic studies.

The relatively narrow defence spectrum of Eva01 contrasts with the broader activity reported for the DUF4062 system Swarożyc (KpSwz) against the BASEL phage collection (Osinski et al., 2026). This difference may reflect distinct trigger-recognition strategies within the broader DUF4062 family. In KpSwz, phage escape mutations map to portal proteins and the AUX region engages phage structural components to activate DUF4062-dependent NADase activity. By contrast, Eva01 escapers repeatedly map to RecA/Sak-like and UvsX-like loci associated with phage DNA metabolism, and Eva01 restricts phage genome accumulation after DNA entry. Thus, although KpSwz and Evangelion proteins may share a conserved DUF4062 effector logic, their activation pathways appear fundamentally different. Notably, both systems require auxiliary (AUX) regions that are essential for defence yet lack recognizable conserved domains. In KpSwz, the AUX region functions as a phage sensor that detects portal-associated structural proteins, whereas our genetic and functional analyses implicate replication-associated processes in Eva01 activation. Together with the extensive sequence diversification observed across Evangelion lineages, these findings suggest that AUX regions may commonly function as sensory modules that determine trigger recognition, while the DUF4062 core provides a conserved defence effector. Portal-associated sensing could permit broad recognition of phages carrying compatible structural determinants, whereas replication-linked sensing may impose stricter requirements on the timing, structure or protein composition of the infection intermediate. This distinction may explain why Eva01 displays pronounced host- and phage-specific activity despite retaining a conserved DUF4062 core.

The broader evolutionary distribution of Evangelion systems supports the idea that bacterial immunity evolves within a highly mobile genetic landscape (Ibarra-Chávez et al., 2022). Recent computational and experimental surveys indicate that currently known defence systems likely represent only a fraction of the bacterial pan-immune repertoire

and that many defence-associated protein families remain functionally uncharacterised (Bernheim and Sorek, 2020; Mordret et al., 2026). Defence systems are pervasive across plasmids, prophages, phage satellites and other MGEs, reflecting ongoing conflicts among phages, bacterial hosts and competing genetic elements (Botelho et al., 2023; Beamud et al., 2024; Pfeifer et al., 2022). In this context, Evangelion appears to represent a mobile defence module that has diversified across distinct evolutionary and ecological settings. Notably, unlike many bacterial immune systems that require multiple proteins for sensing, signalling and interference, Evangelion is encoded by a single gene that combines a conserved DUF4062 effector core with a highly variable auxiliary region. This compact architecture may facilitate HGT and stable maintenance on plasmids and other MGEs, while allowing diversification of trigger-recognition functions through AUX-region evolution.

Recent work has shown that autoimmunity is a major evolutionary constraint on anti-phage defence systems, with increased defence activity often accompanied by increased self-toxicity, thereby favouring regulatory mechanisms that limit basal activity (Aframian et al., 2025). We therefore speculate that the apparent coupling of DUF4062 effector activity to AUX-dependent activation provides an intrinsic layer of self-regulation that minimises basal toxicity and improves compatibility following horizontal transfer into diverse host backgrounds. Such a mechanism could make single-gene systems such as Evangelion less prone to autoimmunity than constitutively active or more complex multi-component systems, while preserving the capacity to evolve highly specialised sensing functions. This evolutionary logic could help explain both the widespread distribution of Evangelion systems and the pronounced lineage-specific differences in phage susceptibility observed across the family. The observation that Eva01 targets staphylococcal *Silviaviruses* whereas Eva03 targets *E. coli Dhillonviruses* further suggests that different Evangelion lineages have adapted to specific host-phage environments while retaining a common DUF4062-based framework. The curated representative Evangelion systems presented in Supplementary Table S1 provide a resource for future comparative analyses of DUF4062-associated defence systems.

Our findings also highlight the value of MGE perturbation as a complementary strategy for defence-system discovery. Most anti-phage systems have been discovered through guilt-by-association approaches that exploit co-localisation with known defence genes or defence islands (Doron et al., 2018; Bernheim and Sorek, 2020). By contrast, Eva01 was identified through a phenotype-first strategy in which removal of a naturally occurring plasmid altered phage susceptibility. This approach enabled the discovery of a single-gene defence system lacking obvious association with canonical defence loci and highlights how experimental interrogation of MGEs can uncover immune functions that remain invisible to current computational frameworks. Given the diversity of MGEs and their central role in shaping bacterial pan-immunity, systematic perturbation of plasmids, prophages and other mobile elements may provide a powerful route for

identifying additional classes of antiviral systems that remain inaccessible to current sequence-based discovery approaches.

In summary, Evangelion reveals how mobile anti-phage immunity can become embedded within the same genetic elements that disseminate antimicrobial resistance. Its association with ARG-containing plasmids, activity against lytic phages in MRSA and diversification across bacterial hosts and MGEs connect plasmid ecology with phage susceptibility. More broadly, our findings suggest that the selective landscape of antimicrobial-resistance plasmids extends beyond antibiotics: by carrying anti-phage defence, these elements can also alter how their bacterial hosts respond to viral predation. Understanding how antibiotic selection, phage predation and horizontal transfer jointly shape such plasmids will be important for defining the evolutionary forces that maintain antimicrobial resistance and bacterial immunity in microbial populations.

Acknowledgements

Authors would like to thank Iñigo Lasa for *S. aureus* Mw2 pMw2 cured strain. We thank Mads F. Hansen, Andreas Haag, Malcolm White, and Janine Z. Bowring for helpful discussions and Andy Millard for helping with Nanopore sequencing of ϕMR003 escaper phages. We also thank Thorsten Gravert from Cmbio for his help with analysis and interpretation of the metabolomics data. Finally, we would like to thank Anette Hørdum Løth and Ayoe Lüchau for all their assistance in the laboratory.

This work was supported by research grants Villum Experiment (VIL58733- Weaponizable satellites) from Villum Foundation, and a JSPS Fellowship (PE24040) to R.I-C., JSPS KAKENHI (No. 25K21732) from Japan Society for the Promotion of Science (JSPS) to K.K.

Author contributions

Conceptualisation, R.I.-C.; Methodology, R.I.-C., A.H.A., K.C., A.M.D., K.A.G., A.T., and K.K.; Investigation, R.I.-C., A.H.A., K.C., A.M.D., K.A.G., A.T., T.S.-P.; Formal Analysis, R.I.-C., K.C., A.H.A., A.M.D., and K.K.; Data Curation, R.I.-C., K.C., and A.M.D.; Visualisation, R.I.-C., A.H.A., K.C., and A.M.D.; Supervision, R.I.-C., J.S.M., and K.K.; Funding Acquisition, R.I.-C. and K.K.; Writing - Original Draft, R.I.-C.; Writing - Review & Editing, all authors

Declaration of interests

No interests are declared.

Data and materials availability

All materials developed in this study will be made available upon request.

Declaration of AI-assisted technologies in the manuscript preparation process

All scripts, analyses and outputs used in this study were independently reviewed, validated and, where necessary, modified by the authors. Generative AI tools were not used to generate experimental data, images or figures, or to make scientific conclusions. The authors take full responsibility for the analyses and content of the manuscript.

Figures

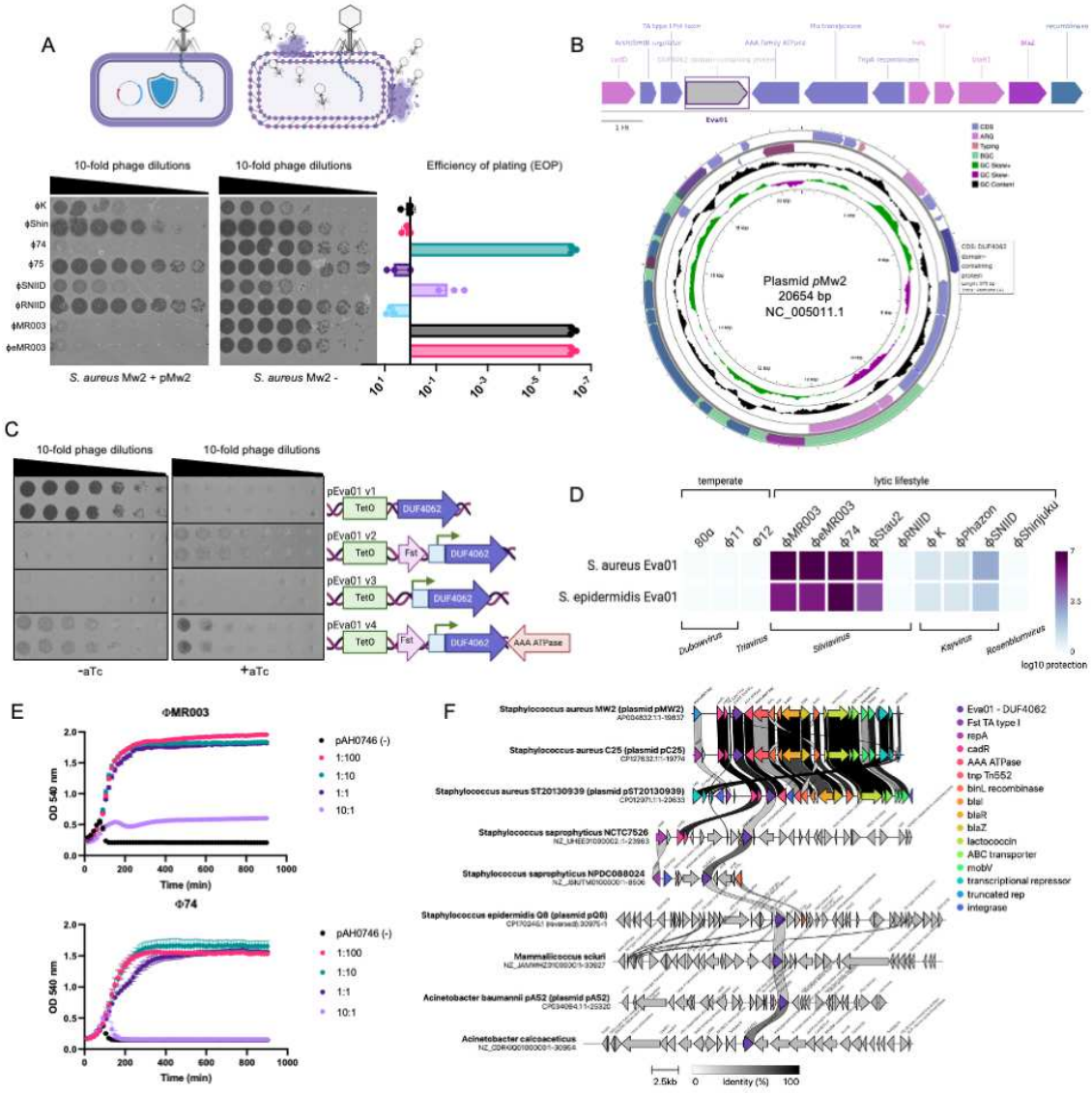


Figure 1. A native MRSA plasmid encodes Evangelion and protects against lytic Silviavirus phages. **(A)** Loss of the native MRSA plasmid pMw2 increases susceptibility to multiple *Silviavirus* phages, as measured by spot assays, efficiency of plating (EOP) (*n*=3 ± SD)**. (B)** Genetic organisation of pMw2 showing the location of Eva01 adjacent to antimicrobial-resistance and mobility-associated genes. **(C)** Mapping of the minimal functional Eva01 locus using inducible constructs containing different DUF4062-containing regions. Representative spot assays are shown**. (D)** Defence spectrum (*n*=4) of Eva01 homologues from different bacterial hosts against a panel of staphylococcal phages. Heatmap colours indicate the magnitude of protection. **(E)** Growth curves (*n*=3) following infection with ϕMR003 or ϕ74 at the indicated phage:bacterium ratios (MOIs). **(F)** Comparative genomic organisation of representative Eva01-containing loci from diverse plasmids. Conserved Eva01 genes are highlighted and neighbouring resistance, mobility and accessory genes are shown. See also Figures S1-S4.

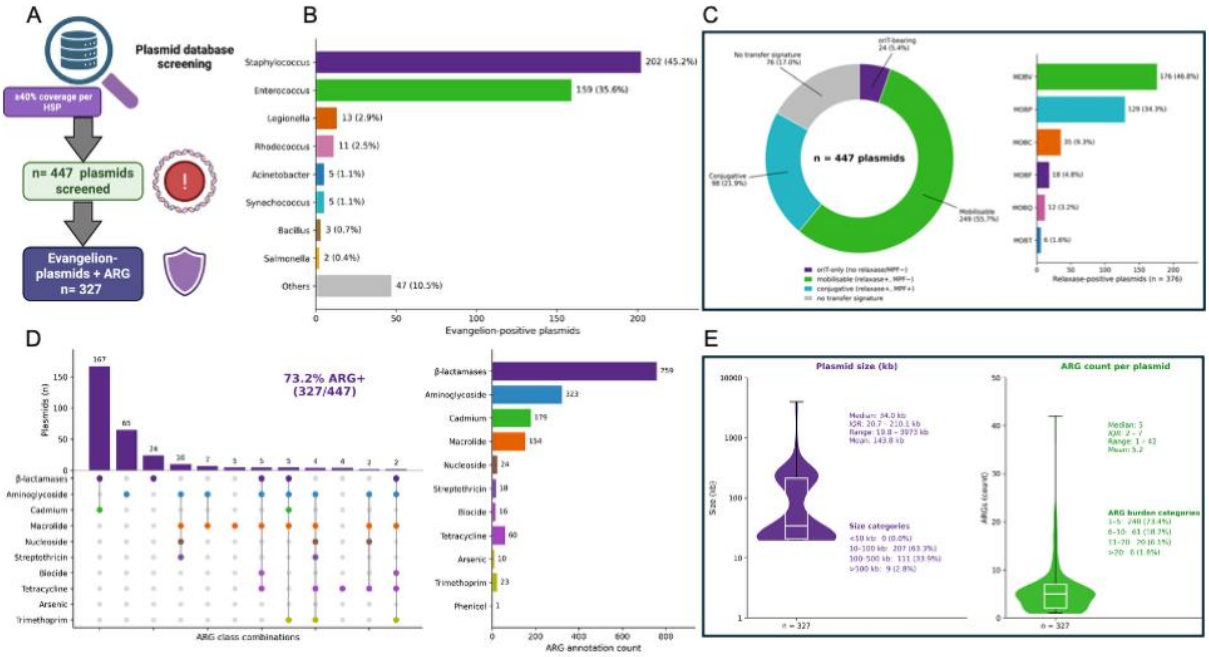


Figure 2. Evangelion type I (Eva01) is widespread on ARG-rich plasmids. (A) Workflow used to identify Eva01-positive plasmids from PLSDB and quantify associated antimicrobial-resistance genes (ARGs). **(B)** Taxonomic distribution of ARG-positive Evangelion plasmids across bacterial genera. **(C)** Distribution of transfer-associated features among ARG-positive Evangelion plasmids. Left, classification of plasmids according to predicted mobility signatures (oriT-bearing, mobilisable, conjugative, or lacking detectable transfer features). Right, distribution of relaxase families among relaxase-positive plasmids. **(D)** Most frequent ARG combinations and resistance classes identified on Evangelion-positive plasmids. **(E)** Distribution of plasmid sizes and ARG content among ARG-positive Evangelion plasmids. Violin plots indicate the distribution of plasmid sizes and ARG counts, with embedded boxplots showing medians and interquartile ranges.

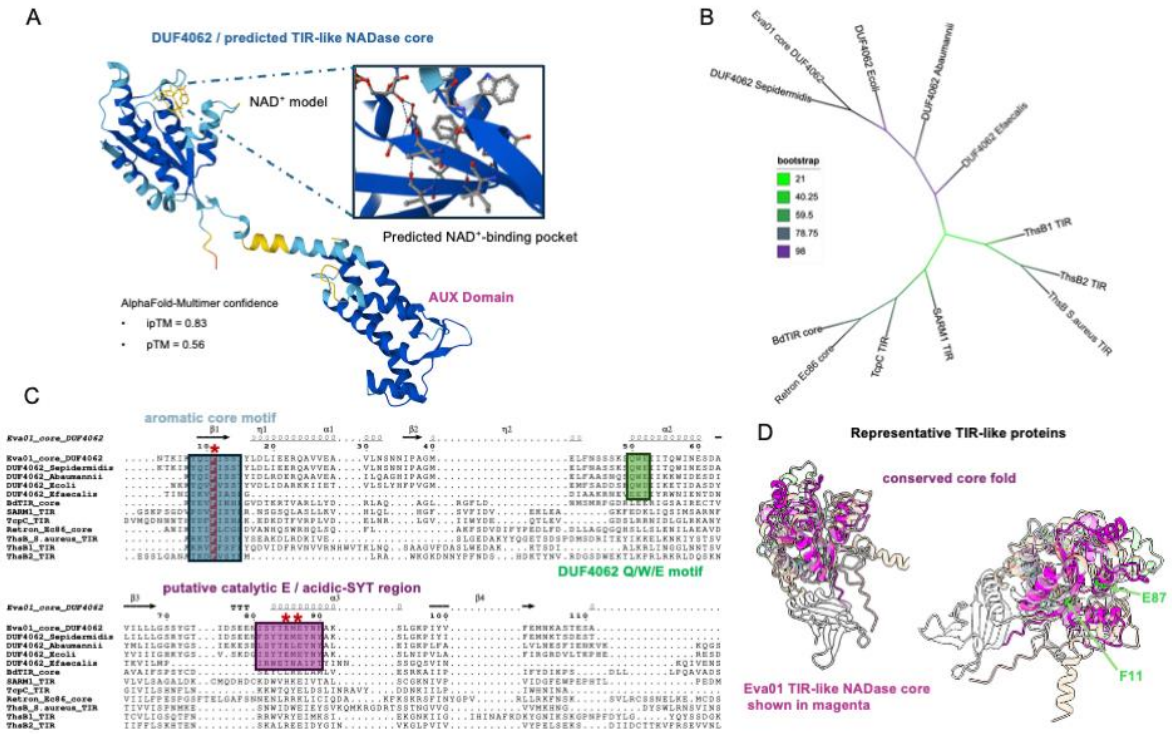


Figure 3. Evangelion proteins contain a conserved DUF4062/TIR-like nucleotide-associated core. (A) AlphaFold3 model and domain organization of representative Eva01 proteins. The N-terminal DUF4062/ TIR-like NADase core is shown with a zoomed view of a predicted NAD^+-binding pocket**. (B)** Maximum-likelihood tree of selected Eva/DUF4062 cores and representative TIR-like proteins. Branch colours indicate bootstrap support. **(C)** Multiple sequence alignment of selected Eva/DUF4062 cores and representative TIR-like proteins. Highlighted regions indicate a conserved aromatic core motif, a DUF4062 Q/W/E motif, and an acidic-SYT region containing the putative catalytic Glu. Red asterisks mark residues selected for mutagenesis. **(D)** Structural superposition of Eva01 with representative TIR-like proteins, showing conservation of the core fold. Eva01 is shown in magenta, with F11 and E87 indicated. See also Figures S5-6.

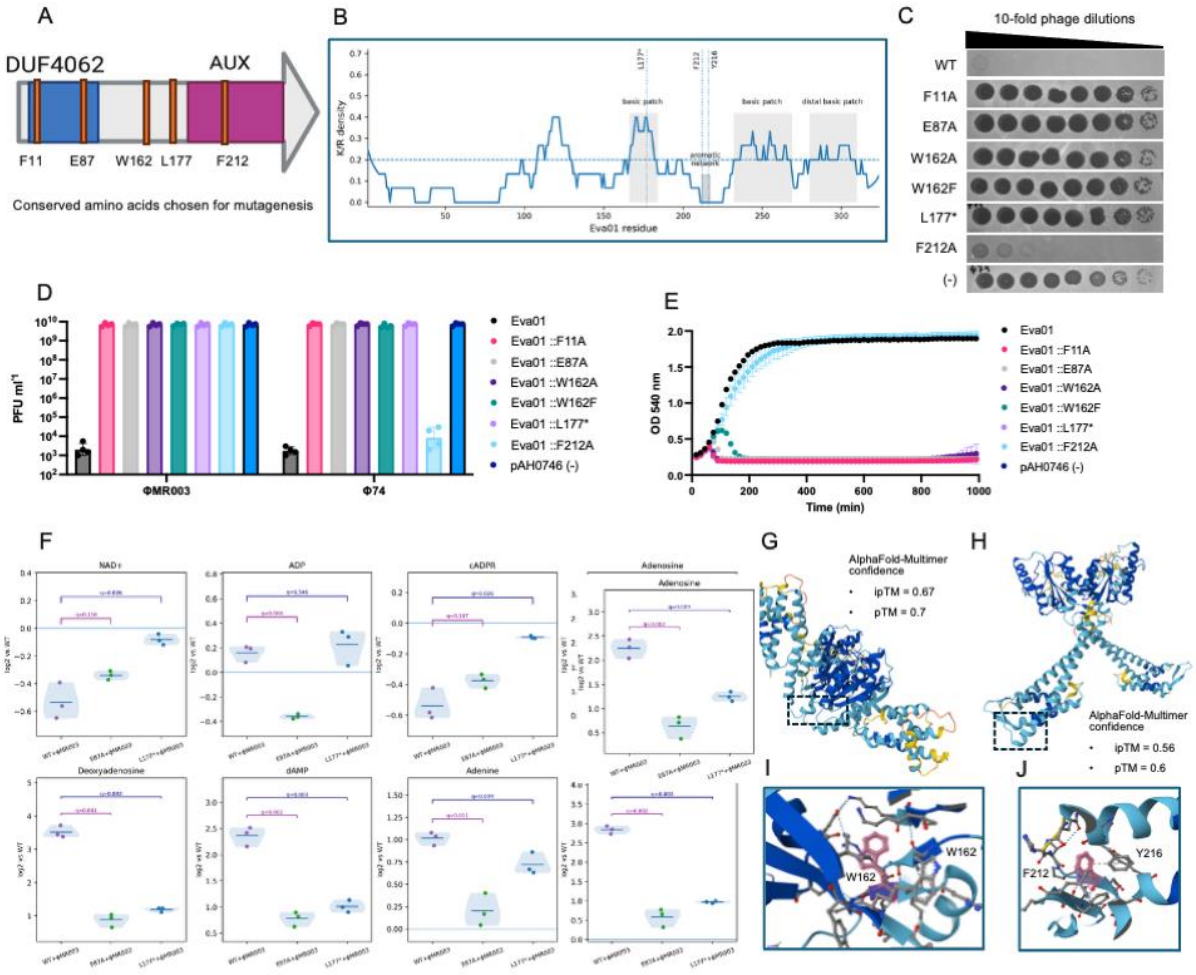


Figure 4. Anti-phage defence requires cooperation between the DUF4062 core and AUX region. (A) Schematic of Eva01 variants targeting conserved DUF4062 residues, the DUF4062-AUX interface and the AUX region. **(B)** Evolutionary conservation and residue-selection strategy used for mutagenesis. Conserved residues selected for functional analysis are indicated. **(C)** Representative spot assays showing the effect of Eva01 mutations on defence against *Silviavirus* phages. **(D)** Quantification of phage propagation (*n*=4 ± SD) following infection with ϕMR003 and ϕ74. **(E)** Liquid infection assays (*n*=3) demonstrating the effects of DUF4062 and AUX mutations on protection against ϕMR003. **(F)** Untargeted LC-MS analysis (*n*=3 ± SD) of selected adenine-associated metabolites following ϕMR003 infection in strains expressing wild-type or mutant Eva01 variants. **(G-H)** AlphaFold3 models of Eva01 oligomeric assemblies. **(I-J)** Structural views highlighting conserved residues W162 and F212 within the predicted DUF4062-AUX interface and associated pockets. See also Figure S7.

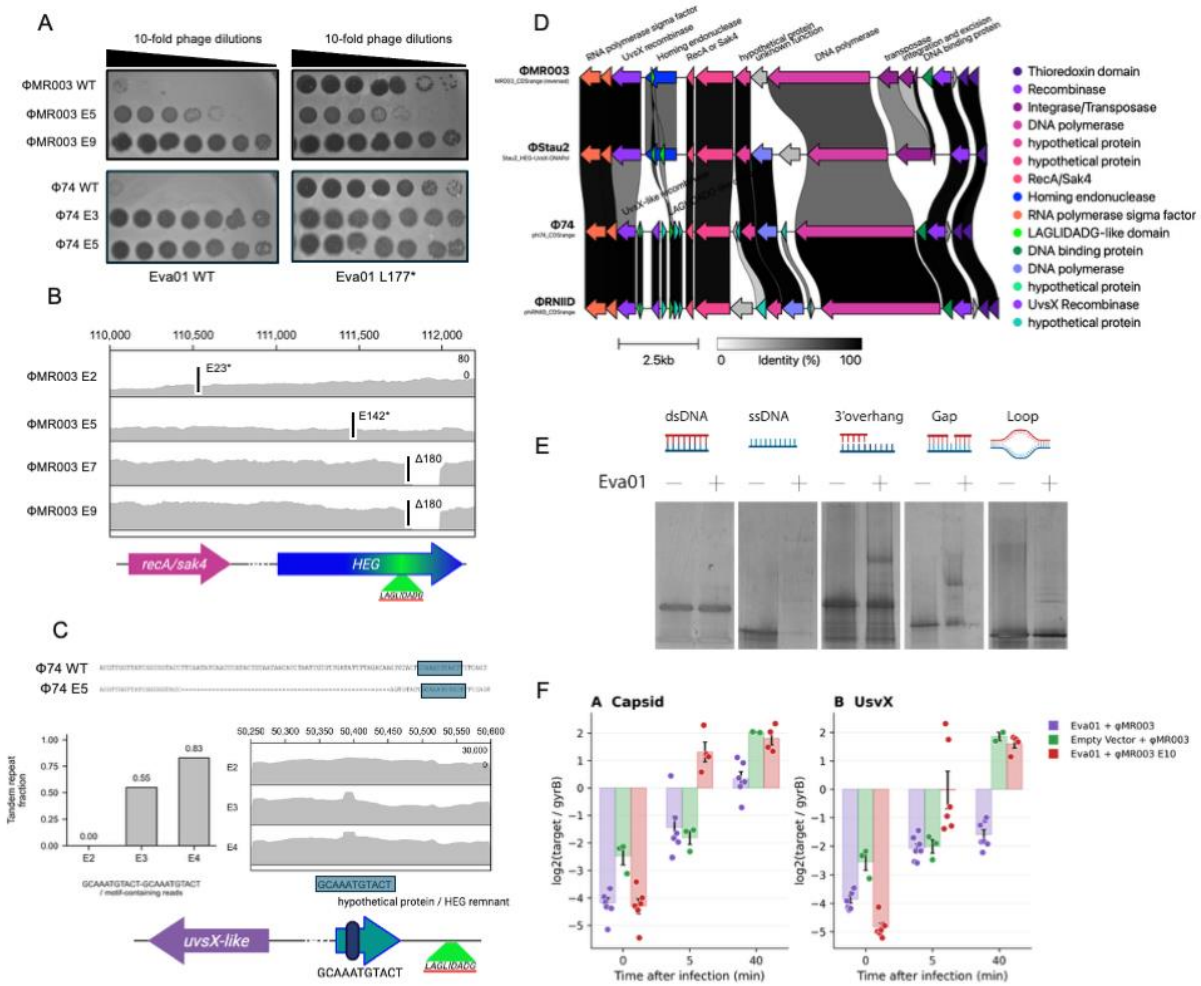


Figure 5. Phage escapers reveal replication-associated triggers of Evangelion defence. (A) Isolation of spontaneous ϕMR003 and ϕ74 escaper mutants capable of infecting Eva01-expressing cells. **(B)** Genomic locations of mutations identified in independent ϕMR003 escapers. **(C)** Genomic locations of mutations identified in independent ϕ74 escapers. **(D)** Comparative analysis of *Silviavirus* genomes showing that escaper mutations converge on a conserved module enriched in recombination- and replication-associated genes, including RecA/Sak-like and UvsX-like proteins. **(E)** Electrophoretic mobility shift assay (EMSA) of purified Eva01 with different DNA substrates. Approximately 15 nM DNA substrate was incubated with 16 nM Eva01 for 40 min before separation on native PAGE. Eva01 preferentially shifted the 3' overhang substrate, with weaker binding to gapped DNA and minimal or no detectable interaction with blunt dsDNA, ssDNA or bubble DNA. **(F)** Digital PCR quantification of intracellular phage DNA following infection with wild-type ϕMR003 or the escaper mutant ϕMR003 E10. Phage capsid and *uvs*X copy numbers were normalized to the chromosomal reference gene *gyr*B and plotted as log2(target/*gyr*B). Bars indicate the mean ± SD, and points $n \geq 3$ independent biological replicates per condition. See also Figures S8-9.

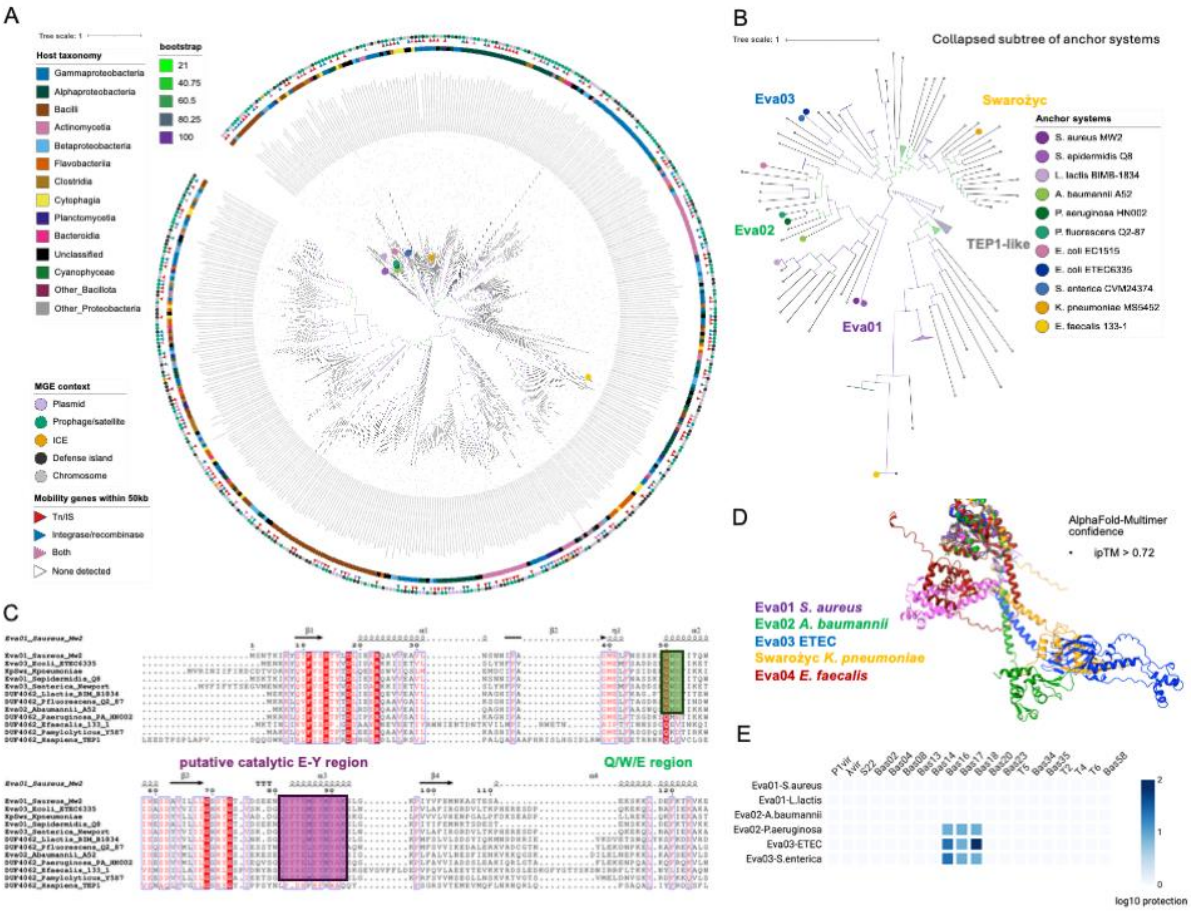


Figure 6. Evangelion systems form diverse defence lineages within the broader DUF4062 protein family. (A) Phylogenetic distribution of approximately 6,000 DUF4062-containing proteins across bacterial genomes and MGEs. Metadata tracks indicate taxonomic origin and genomic context. **(B)** Expanded view of major DUF4062-associated lineages, including Evangelion types Eva01-Eva04, together with the related Swarożyc and TEP1-like proteins. **(C)** Alignment of representative Evangelion proteins highlighting conservation of the putative catalytic E-Y region and DUF4062 Q/W/E motif. **(D)** Structural comparison of representative Evangelion proteins from diverse bacterial hosts showing conservation of the DUF4062 core despite divergence of auxiliary regions. **(E)** Defence profiles of representative Evangelion systems against host-specific phage panels. Heatmap colours indicate the magnitude of protection. See also Figure S10.

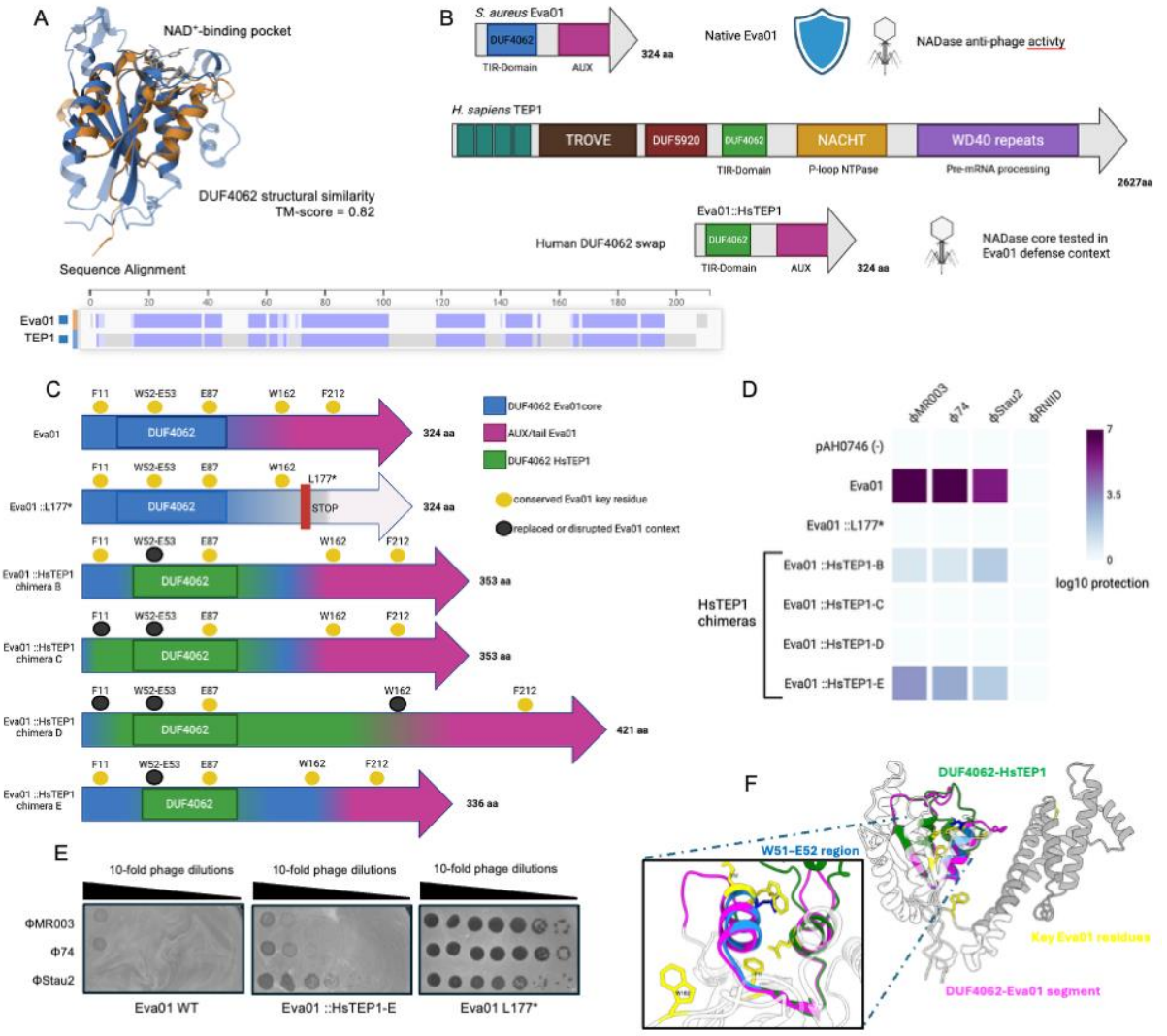


Figure 7. Human TEP1 DUF4062 fragments partially substitute for the Evangelion core. (A) Structural comparison and sequence alignment of Eva01 and the DUF4062/TIR-like region of human TEP1. **(B)** Design rationale for replacing Eva01 DUF4062 segments with the corresponding HsTEP1 region while retaining the Eva01 AUX/tail. **(C)** Schematic of Eva01::HsTEP1 chimeras. Yellow circles indicate conserved/key Eva01 residues or motifs, whereas black circles indicate regions in which the native Eva01 context is replaced or altered. **(D)** Heatmap of phage protection by Eva01, Eva01 L177*, and HsTEP1 chimeras. **(E)** Representative spot assays showing strong Eva01 defence, partial activity of Eva01::HsTEP1-E, and loss of defence in Eva01 L177*. **(F)** AlphaFold model overlay of Eva01 WT and Eva01::HsTEP1-E. The native Eva01 DUF4062 segment is shown in magenta, the HsTEP1-derived segment in green, and key Eva01 residues in yellow. The E chimera preserves the overall core architecture but alters the local W51-E52/Q-W-E region, consistent with partial rather than complete functional rescue. See also Figures S11-12.

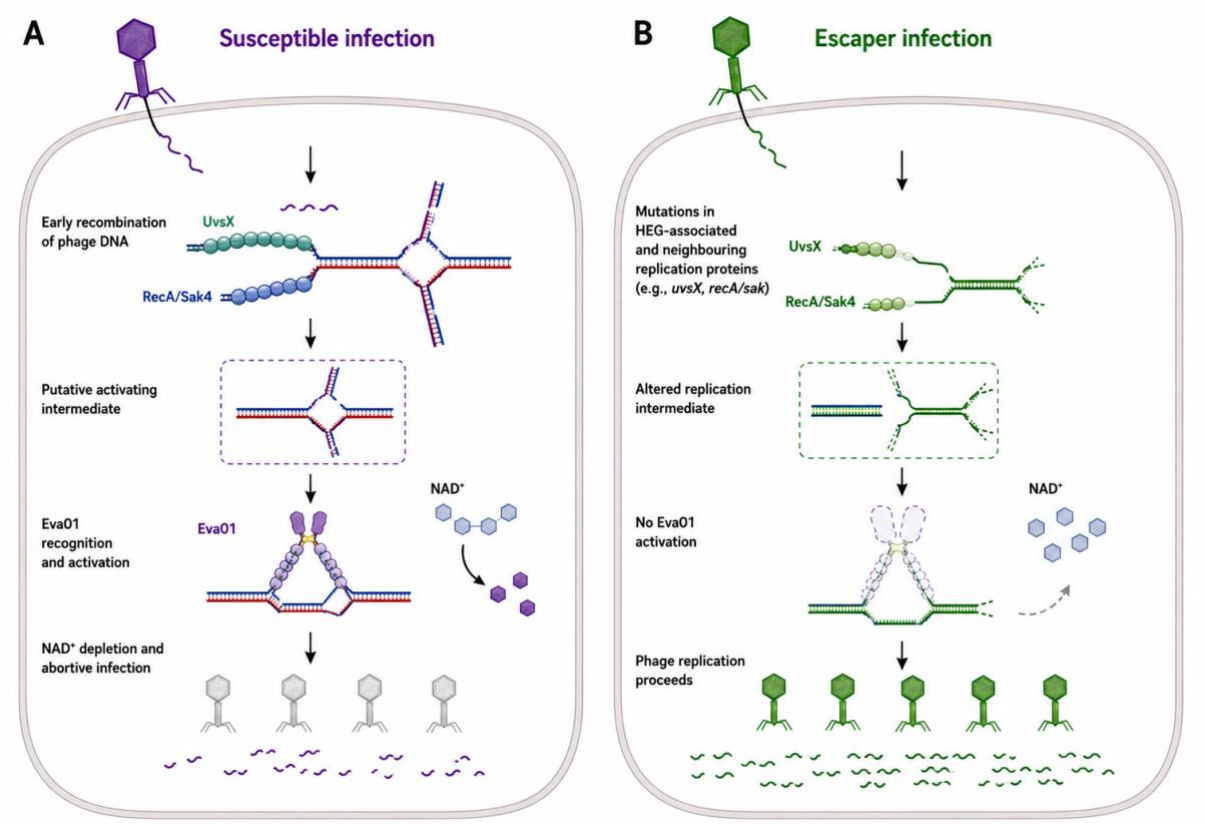


Figure 8. A model for Evangelion type 1 sensing of replication-associated phage intermediates. (A) During susceptible infection, phage recombination and replication generate UvsX- and RecA/Sak-like processes and associated DNA intermediates proposed to promote Eva01 activation. Activation of the DUF4062 defence protein triggers NAD^+ depletion and abortive infection, restricting productive phage replication. **(B)** Escaper mutations in HEG-associated functions and neighbouring replication genes may alter the activating process or intermediate, thereby allowing escape from Eva01 defence.

References

Abramson, J., Adler, J., Dunger, J., Evans, R., Green, T., Pritzel, A., Ronneberger, O., Willmore, L., Ballard, A.J., Bambrick, J., et al. (2024). Accurate structure prediction of biomolecular interactions with AlphaFold 3. Nature 630, 493–500. https://doi.org/10.1038/s41586-024-07487-w.

Aframian, N., Omer Bendori, S., Hen, T., Guler, P., and Eldar, A. (2025). Expression level of anti-phage defence systems controls a trade-off between protection range and autoimmunity. Nat. Microbiol. 10, 1954–1962. https://doi.org/10.1038/s41564-025-02063-y.

Aguayo-González, A., Martínez-Flores, I., Bustos, P., Santamaría, R.I., Cabrera-Contreras, R., Martínez-Gamboa, A., Ibarra-Chávez, R., and González, V. (2026). Predicted and inducible prophages display contrasting virulence gene profiles within the prophage–SaPI mobilome of Staphylococcus aureus. mSphere 11, e00103-26. https://doi.org/10.1128/msphere.00103-26.

Ares-Arroyo, M., Coluzzi, C., and Rocha, E.P.C. (2023). Origins of transfer establish networks of functional dependencies for plasmid transfer by conjugation. Nucleic Acids Res. 51, 3001–3016. https://doi.org/10.1093/nar/gkac1079.

Askarian, F., van Sorge, N.M., Sangvik, M., Beasley, F.C., Henriksen, J.R., Sollid, J.U.E., van Strijp, J.A.G., Nizet, V., and Johannessen, M. (2014). A Staphylococcus aureus TIR domain protein virulence factor blocks TLR2-mediated NF-κB signaling. J. Innate Immun. 6, 485–498. https://doi.org/10.1159/000357618.

Beamud, B., Ibáñez de Opakua, A., Maharjan, R., and Penadés, J.R. (2024). Going viral: The role of mobile genetic elements in bacterial immunity. Cell Host Microbe 32, 804–819. https://doi.org/10.1016/j.chom.2024.05.009.

Bernheim, A., and Sorek, R. (2020). The pan-immune system of bacteria: antiviral defence as a community resource. Nat. Rev. Microbiol. 18, 113–119. https://doi.org/10.1038/s41579-019-0278-2.

Bondy-Denomy, J., Qian, J., Westra, E.R., Buckling, A., Guttman, D.S., Davidson, A.R., and Maxwell, K.L. (2016). Prophages mediate defense against phage infection through diverse mechanisms. ISME J. 10, 2854–2866. https://doi.org/10.1038/ismej.2016.79.

Botelho, J., Jang, H.B., Liu, X., and Roberts, A.P. (2023). Defense systems are pervasive across chromosomally integrated mobile genetic elements and are inversely correlated to virulence and antimicrobial resistance. Nucleic Acids Res. 51, 4385–4397. https://doi.org/10.1093/nar/gkad282.

Cazares, A., Figueroa, W., Cazares, D., Lima, L., Turnbull, J.D., et al. (2025). Pre- and postantibiotic epoch: The historical spread of antimicrobial resistance. Science 390, eadr1522. https://doi.org/10.1126/science.adr1522.

Chihara, K., Azam, A.H., Egorov, A.A., et al. (2026). Phage homing endonuclease amplifies anti-defense genes to evade bacterial immunity. Nat. Commun. 17, 3468. https://doi.org/10.1038/s41467-026-71036-4.

Cui, W., Fendley, J.M., Srikant, S., and Shraiman, B.I. (2025). A minimal model of panimmunity maintenance by horizontal gene transfer in the ecological dynamics of bacteria and phages. Proc. Natl. Acad. Sci. U.S.A. 122(31), e2417628122. https://doi.org/10.1073/pnas.2417628122

Dedrick, R.M., Jacobs-Sera, D., Bustamante, C.A.G., Garlena, R.A., Mavrich, T.N., Pope, W.H., Reyes, J.C.C., Russell, D.A., Adair, T., Alvey, R., et al. (2017). Prophage-mediated defence against viral attack and viral counter-defence. Nat. Microbiol. 2, 16251. https://doi.org/10.1038/nmicrobiol.2016.251.

Dorado-Morales, P., Garcillán-Barcia, M.P., Lasa, I., and Solano, C. (2021). Fitness cost evolution of natural plasmids of Staphylococcus aureus. mBio 12, e03094-20. https://doi.org/10.1128/mBio.03094-20.

Doron, S., Melamed, S., Ofir, G., Leavitt, A., Lopatina, A., Keren, M., Amitai, G., and Sorek, R. (2018). Systematic discovery of antiphage defense systems in the microbial pangenome. Science 359, eaar4120. https://doi.org/10.1126/science.aar4120.

Essuman, K., Summers, D.W., Sasaki, Y., Mao, X., DiAntonio, A., and Milbrandt, J. (2017). The SARM1 Toll/interleukin-1 receptor domain possesses intrinsic NAD+ cleavage activity that promotes pathological axonal degeneration. Neuron 93, 1334–1343.e5. https://doi.org/10.1016/j.neuron.2017.02.022.

Fillol-Salom, A., Rostøl, J.T., Ojiogu, A.D., Chen, J., Douce, G., Humphrey, S., and Penadés, J.R. (2022). Bacteriophages benefit from mobilizing pathogenicity islands encoding immune systems against competitors. Cell 185, 3248–3262.e20. https://doi.org/10.1016/j.cell.2022.07.014.

Firth, N., Jensen, S.O., Kwong, S.M., Skurray, R.A., and Ramsay, J.P. (2018). Staphylococcal plasmids, transposable and integrative elements. Microbiol. Spectr. 6, GPP3-0030-2018. https://doi.org/10.1128/microbiolspec.GPP3-0030-2018.

Frost, L.S., Leplae, R., Summers, A.O., and Toussaint, A. (2005). Mobile genetic elements: The agents of open source evolution. Nat. Rev. Microbiol. 3, 722–732. https://doi.org/10.1038/nrmicro1235.

GBD 2021 Antimicrobial Resistance Collaborators. (2024). Global burden of bacterial antimicrobial resistance 1990–2021: A systematic analysis with forecasts to 2050. Lancet 404, 1199–1226. https://doi.org/10.1016/S0140-6736(24)01867-1.

Grafakou, A., Mosterd, C., Beck, M.H., Kelleher, P., McDonnell, B., de Waal, P.P., van Rijswijck, I.M.H., van Peij, N.N.M.E., Cambillau, C., Mahony, J., and van Sinderen, D. (2024). Discovery of antiphage systems in the lactococcal plasmidome. Nucleic Acids Res. 52, 9760–9776. https://doi.org/10.1093/nar/gkae671.

Horsefield, S., Burdett, H., Zhang, X., Manik, M.K., Shi, Y., Chen, J., Qi, T., Gilley, J., Lai, J.S., Rank, M.X., et al. (2019). NAD+ cleavage activity by animal and plant TIR domains in cell death pathways. Science 365, 793–799. https://doi.org/10.1126/science.aax1919.

Hossain, M., Aslan, B., and Hatoum-Aslan, A. (2024). Tandem mobilization of anti-phage defenses alongside SCCmec elements in staphylococci. Nat. Commun. 15, 8820. https://doi.org/10.1038/s41467-024-53146-z.

Humphrey, S., San Millán, Á., Toll-Riera, M., Connolly, J., Flor-Duro, A., Chen, J., et al. (2021). Staphylococcal phages and pathogenicity islands drive plasmid evolution. Nat. Commun. 12, 5845. https://doi.org/10.1038/s41467-021-26101-5.

Ibarra-Chávez, R., Brady, A., Chen, J., Penadés, J.R., and Haag, A.F. (2022). Phage-inducible chromosomal islands promote genetic variability by blocking phage reproduction and protecting transductants from phage lysis. PLoS Genet. 18, e1010146. https://doi.org/10.1371/journal.pgen.1010146.

Ipoutcha, T., Wang, Y., Rocha, E.P.C., and Penadés, J.R. (2026). Mobile genetic elements drive a fusion-deletion life cycle that shapes plasmid evolution and antimicrobial resistance. bioRxiv. https://doi.org/10.64898/2026.01.09.696371.

Ka, D., Oh, H., Park, E., Kim, J.-H., and Bae, E. (2020). Structural and functional evidence of bacterial antiphage protection by Thoeris defense system via NAD+ degradation. Nat. Commun. 11, 2816. https://doi.org/10.1038/s41467-020-16703-w.

Kuang, X., Gorzynski, J., Touchon, M., Shkoporov, A., Rocha, E.P.C., Fitzgerald, J.R., Chen, J., Rostøl, J.T., and Penadés, J.R. (2026). Bacteriophages mobilize bacterial defense systems via lateral transduction. Sci. Adv. 12, eadx5749. https://doi.org/10.1126/sciadv.adx5749.

Lapin, D., Johanndrees, O., Wu, Z., Li, X., and Parker, J.E. (2022). Molecular innovations in plant TIR-based immunity signaling. Plant Cell 34, 1479–1496. https://doi.org/10.1093/plcell/koac035.

Leavitt, A., Yirmiya, E., Amitai, G., Lu, A., Garb, J., Herbst, E., Morehouse, B.R., Hobbs, S.J., Antine, S.P., Sun, Z.-Y.J., et al. (2022). Viruses inhibit TIR gcADPR signalling to

776 overcome bacterial defence. Nature 611, 326–331. https://doi.org/10.1038/s41586-022-
777 05375-9.

778 Lerdsittikul, V., Apiratwarrasakul, S., Atithep, T., Withatanung, P., Indrawattana, N.,
779 Pumirat, P., Chaiwattanarungruengpaisan, S., and Thongdee, M. (2024). Isolation and
780 characterisation of a novel Silviavirus bacteriophage promising antimicrobial agent
781 against methicillin-resistant Staphylococcus aureus infections. Sci. Rep. 14, 9251.
782 https://doi.org/10.1038/s41598-024-59903-w.

783 Maffei, E., Shaidullina, A., Burkolter, M., Heyer, Y., Estermann, F., Druelle, V., Sauer, P.,
784 Willi, L., Michaelis, S., Hibi, H., Thaler, D.S., and Harms, A. (2021) Systematic exploration
785 of Escherichia coli phage–host interactions with the BASEL phage collection. PLOS
786 Biology 19(11): e3001424. https://doi.org/10.1371/journal.pbio.3001424

787 Makarova, K.S., Wolf, Y.I., Snir, S., and Koonin, E.V. (2011). Defense islands in bacterial
788 and archaeal genomes and prediction of novel defense systems. J. Bacteriol. 193, 6039–
789 6056. https://doi.org/10.1128/JB.05535-11.

790 Molano, L.A.G., Galata, V., Fehlmann, T., Backes, C., and Keller, A. (2025). The PLSDB
791 2025 update: Enhanced annotations and improved functionality for comprehensive
792 plasmid research. Nucleic Acids Res. 53, D1847–D1855.
793 https://doi.org/10.1093/nar/gkae1095.

794 Mordret, E., et al. (2026). Protein and genomic language models uncover the unexplored
795 diversity of bacterial immunity. Science 392, eadv8275.
796 https://doi.org/10.1126/science.adv8275.

797 Ofir, G., Herbst, E., Baroz, M., Cohen, D., Millman, A., Doron, S., Tal, N., Malheiro, D.B.A.,
798 Malitsky, S., Amitai, G., et al. (2021). Antiviral activity of bacterial TIR domains via immune
799 signalling molecules. Nature 600, 116–120. https://doi.org/10.1038/s41586-021-04098-
800 7.

801 Osinski, A., Mayro, B., Lopez, V.A., Schrad, J., Choi, H., Tomchick, D.R., Pawlowski, K.,
802 Forsberg, K., Shahmoradian, S.H., and Tagliabracci, V.S. (2026). TIR-like NADases act in
803 bacterial immunity and the RNA vault. bioRxiv.
804 https://doi.org/10.64898/2026.05.01.722283.

805 Partridge, S.R., Kwong, S.M., Firth, N., and Jensen, S.O. (2018). Mobile genetic elements
806 associated with antimicrobial resistance. Clin. Microbiol. Rev. 31, e00088-17.
807 https://doi.org/10.1128/CMR.00088-17.

808 Payne, L.J., Todeschini, T.C., Wu, Y., Perry, B.J., Ronson, C.W., Fineran, P.C., Nobrega, F.L.,
809 and Jackson, S.A. (2021). Identification and classification of antiviral defence systems in
810 bacteria and archaea with PADLOC reveals new system types. Nucleic Acids Res. 49,
811 10868–10878. https://doi.org/10.1093/nar/gkab883.

812 Peng, C., Hanawa, T., Azam, A.H., LeBlanc, C., Ung, P., Matsuda, T., Onishi, H., Miyanaga,
813 K., and Tanji, Y. (2019). Silviavirus phage ϕMR003 displays a broad host range against
814 methicillin-resistant Staphylococcus aureus of human origin. Appl. Microbiol.
815 Biotechnol. 103, 7751–7765. https://doi.org/10.1007/s00253-019-10039-2.

816 Pfeifer, E., Moura de Sousa, J.A., Touchon, M., and Rocha, E.P.C. (2022). When bacteria
817 are phage playgrounds: Interactions between viruses, cells, and MGEs. Curr. Opin.
818 Microbiol. 70, 102230. https://doi.org/10.1016/j.mib.2022.102230.

819 Pinilla-Redondo, R., Russel, J., Mayo-Muñoz, D., Shah, S.A., Garrett, R.A., Nesme, J.,
820 Madsen, J.S., Fineran, P.C., and Sørensen, S.J. (2022). CRISPR-Cas systems are
821 widespread accessory elements across bacterial and archaeal plasmids. Nucleic Acids
822 Res. 50, 4315–4328. https://doi.org/10.1093/nar/gkab859.

823 Roberts, C.G., Fishman, C., Banh, D., and Marraffini, L.A. (2025). Bacterial TIR-based
824 immune systems sense phage capsids to initiate defense. Nat. Microbiol.
825 https://doi.org/10.1038/s41564-025-02150-0.

826 Rodríguez-Beltrán, J., DelaFuente, J., León-Sampedro, R., MacLean, R.C., and San Millán,
827 Á. (2021). Beyond horizontal gene transfer: the role of plasmids in bacterial evolution.
828 Nat. Rev. Microbiol. 19, 347–359. https://doi.org/10.1038/s41579-020-00497-1.

829 Rostøl, J.T., Quiles-Puchalt, N., Iturbe-Sanz, P., Lasa, Í., and Penadés, J.R. (2024).
830 Bacteriophages avoid autoimmunity from cognate immune systems as an intrinsic part
831 of their life cycles. Nat. Microbiol. 9, 1312–1324. https://doi.org/10.1038/s41564-024-
832 01661-6.

833 Rousset, F., Depardieu, F., Miele, S., Dowding, J., Laval, A.-L., Lieberman, E., Garry, D.,
834 Rocha, E.P.C., Bernheim, A., and Bikard, D. (2022). Phages and their satellites encode
835 hotspots of antiviral systems. Cell Host Microbe 30, 740–753.e5.
836 https://doi.org/10.1016/j.chom.2022.02.018.

837 Samuel, B., Mittelman, K., Croitoru, S.Y., Ben Haim, M., and Burstein, D. (2024). Diverse
838 anti-defence systems are encoded in the leading region of plasmids. Nature 635, 186–
839 193. https://doi.org/10.1038/s41586-024-07994-w.

840 San Millan, Á. (2018). Evolution of plasmid-mediated antibiotic resistance in the clinical
841 context. Trends Microbiol. 26, 978–985. https://doi.org/10.1016/j.tim.2018.06.007.

842 Sastre-Dominguez, J., Rodera-Fernandez, P., DelaFuente, J., Martínez-González, S.,
843 Quesada, S., Valencoso-Requena, M., Calvo-Villamañán, A., Costas, C., Fuentes-
844 Hernández, A., Santos-Lopez, A., and San Millán, Á. (2026). Plasmids promote
845 antimicrobial resistance through insertion sequence-mediated gene inactivation. Nat.
846 Microbiol. 11, 976–992. https://doi.org/10.1038/s41564-026-02290-x.

Smillie, C., Garcillán-Barcia, M.P., Francia, M.V., Rocha, E.P.C., and de la Cruz, F. (2010). Mobility of plasmids. Microbiol. Mol. Biol. Rev. 74, 434–452. https://doi.org/10.1128/MMBR.00020-10.

Voss, S.M., King, K.C., Hunt, D.J., Wilson, A.A., Samuel, B., Bagno, O.R., Sparklin, P.F.W., Cassata, B., and Modell, J.W. (2026). Engineered phages evade the complete defense repertoire of highly phage-resistant MRSA clinical isolates. bioRxiv. https://doi.org/10.64898/2026.03.26.714447.

Wan, L., Essuman, K., Anderson, R.G., Sasaki, Y., Monteiro, F., Chung, E.-H., Nishimura, E.O., DiAntonio, A., Milbrandt, J., Dangl, J.L., and Nishimura, M.T. (2019). TIR domains of plant immune receptors are NAD+-cleaving enzymes that promote cell death. Science 365, 799–803. https://doi.org/10.1126/science.aax1771.

Wang, J., Chitsaz, F., Derbyshire, M.K., Gonzales, N.R., Gwadz, M., Lu, S., Marchler, G.H., Song, J.S., Thanki, N., Yamashita, R.A., et al. (2023). The conserved domain database in 2023. Nucleic Acids Res. 51, D384–D388. https://doi.org/10.1093/nar/gkac1096.

Wang, S., et al. (2024). The role of TIR domain-containing proteins in bacterial defense against phages. Nat. Commun. 15, 7384. https://doi.org/10.1038/s41467-024-51738-3.

Yirmiya, E., Leavitt, A., Hurieva, B., Falkovich, A.H., Béchon, N., Rousset, F., Osterman, I., and Sorek, R. (2025). Systematic discovery of TIR-based immune signaling systems in bacteria. bioRxiv. https://doi.org/10.64898/2025.12.03.692087.

Zheng, H., Payne, L., He, W., Mestre, M.R., Yang, L., Dechesne, A., Pinilla-Redondo, R., Nesme, J., and Sørensen, S.J. (2026). Plasmids as persistent genetic reservoirs of bacterial defense systems in wastewater treatment. Microbiome 14, 50. https://doi.org/10.1186/s40168-025-02297-2.

Methods

Bacterial strains and growth conditions

Bacterial strains, plasmids and bacteriophages used in this study are listed in Supplementary Table S3. *Escherichia coli* strains were grown in lysogeny broth (LB) at 37°C with shaking at 180 rpm or on LB agar plates. When required, ampicillin was used at 100 µg mL-1.

Staphylococcus aureus strains were grown in tryptic soy broth (TSB) at 37°C with shaking at 180 rpm or on tryptic soy agar (TSA) plates. When required, erythromycin and chloramphenicol were used at 10 µg mL-1.

Bacteriophages

Bacteriophages used in this study are listed in Supplementary Table S3. Phages were propagated on the indicated permissive host strains using phage base top-agar (PTA) overlay methods. Phage lysates were filtered to remove bacterial cells and stored in phage buffer at 4°C.

Plasmid construction and transformation

All bacterial strains, plasmids, bacteriophages and oligonucleotides used in this study are listed in Supplementary Tables S3 and S4. The tetracycline-inducible Staphylococcus shuttle vector pAH0746, kindly provided by Andreas Haag, was used for heterologous expression in *S. aureus*. pLI50 was used as an additional shuttle vector where indicated. For experiments in Gram-negative bacteria, Evangelion homologues were cloned into the arabinose-inducible *E. coli* expression vector pKLC23 or the tetracycline-inducible pAH0746 vector. For *P. aeruginosa,* we used the tetracycline-inducible expression vector pKCN-276, as appropriate. Recombinant Eva01 used for biochemical characterisation was expressed from pET-28a(+), generating an N-terminal His_6-tagged fusion protein.

The Eva01 coding sequence and its variants were amplified from *S. aureus* Mw2 genomic DNA. The *S. epidermidis* Eva01 homologue was amplified from strain pQ8, kindly provided by Jonathan C. Thomas. Evangelion homologues from *Acinetobacter baumannii*, *Lactococcus lactis*, *Pseudomonas aeruginosa*, *Escherichia coli*, and *Salmonella enterica* were synthesised commercially (Twist Bioscience). Site-directed mutants, truncation variants and chimeric constructs were generated by overlap-extension PCR using mutagenic primers. All constructs were assembled into the appropriate vector backbone using the NEBuilder HiFi DNA Assembly Master Mix (New England Biolabs) according to the manufacturer's instructions.

Recombinant plasmids were propagated by chemical transformation into *E. coli* IM08B or IM01B, depending on the *S. aureus* clonal complex bypass required (Monk et al., 2015).

Plasmid sequences were verified by Sanger sequencing (Eurofins Genomics) before transformation into the appropriate bacterial host. pAH0746- and pLI50-derived plasmids were introduced into sucrose-electrocompetent *S. aureus* RN4220 (CC8) or Mw2 (CC1) by electroporation. pKLC23- and pET-28a-derived constructs were transformed into the indicated *E. coli* MG1655 or IM08B by chemical transformation. Transformants were selected on the appropriate antibiotic-containing media.

Phage spot assays

Overnight cultures of *S. aureus* carrying either the empty pAH0746 vector or the indicated Evangelion constructs were diluted 1:50 into fresh tryptic soy broth (TSB) containing the appropriate antibiotic and grown to an OD_{540} of approximately 0.4. Where indicated, Evangelion expression was induced with anhydrotetracycline (aTc; 50 ng mL^{-1}) added at the time of inoculation. Bacterial lawns were prepared by mixing 300 µL of culture with molten phage top agar (PTA; 20 g L^{-1} Nutrient Broth No. 2, Oxoid, 3.5 g L^{-1} agar, supplemented with 10 mM $CaCl_2$) before pouring onto TSA plates supplemented with the appropriate antibiotic. Phage lysates were serially diluted in phage buffer (50 mM Tris-HCl, pH 8.0, 100 mM NaCl, 1 mM $MgSO_4$ and 4 mM $CaCl_2$), and 5-10 µL of each dilution was spotted onto bacterial lawns. Plates were incubated overnight at 37°C.

For phage spot assays performed with the BASEL bacteriophage collection (Maffei et al., 2021) and additional Coli phages, *E. coli* MG1655 carrying Evangelion homologues expressed from either the arabinose-inducible pKLC23 vector or the tetracycline-inducible pAH0746 vector were grown overnight in LB supplemented with the appropriate antibiotic, diluted 1:50 into fresh LB and grown to mid-exponential phase. Gene expression was induced with either L-arabinose 0.2% (w/v) (pKLC23) or aTc 100 ng mL^{-1} (pAH0746), as indicated. Bacterial lawns were prepared using molten LB top agar and LB agar plates supplemented with the appropriate antibiotic, and phage spot assays were performed as described above.

For experiments in *P. aeruginosa* PAO1 Δprophages, the Evangelion homologue was expressed from the tetracycline-inducible vector pKCN-276 under control of the TetO promoter. Overnight cultures were grown in LB containing the appropriate antibiotic, diluted 1:50 into fresh medium and induced with 100 ng mL^{-1} anhydrotetracycline before preparation of bacterial lawns. Phage spot assays were subsequently performed as described above using LB top agar and the corresponding *P. aeruginosa* phages.

Protection was calculated by comparing plaque formation on strains expressing Evangelion constructs with the corresponding empty-vector control.

Efficiency of plating assays

Efficiency of plating (EOP) was determined by plating serial dilutions of phage lysates onto bacterial lawns carrying either the empty vector or the indicated Evangelion construct. Plaques were enumerated following overnight incubation at 37°C, and EOP was calculated as the ratio of plaque-forming units (PFU mL^{-1}) recovered on the defence-containing strain relative to the empty-vector control.

Liquid infection assays

Overnight cultures were diluted 1:50 into fresh TSB supplemented with the appropriate antibiotics and grown to early exponential phase. Where indicated, expression of Eva01 or derivative constructs was induced with anhydrotetracycline (aTc; 50 ng mL^{-1}). Cultures were infected with the indicated bacteriophages at the multiplicities of infection described in the corresponding figure legends, and bacterial growth was monitored by measuring optical density at 540 nm (OD_{540}).

For high-resolution growth curves, overnight cultures were diluted 1:50 into fresh TSB and grown to early exponential phase before being normalized to an OD_{540} of 0.1. Aliquots were dispensed into sterile 96-well microplates, and bacteriophages were added as indicated. Plates were incubated at 37°C in a BioTek ELx808 microplate reader (BioTek Instruments) with continuous orbital shaking (500 rpm), and OD_{540} measurements were recorded every 10 min. Where indicated, cultures were recovered at the end of the experiment for phage titration by standard plaque assay.

Identification of Eva01-positive plasmids

A panel of bacterial Eva01/DUF4062 protein sequences, including Eva01 from *S. aureus* Mw2, was used to query the PLSDB database (Molano et al., 2025; release 2024_05_31_v2) using the sequence-similarity tBLASTn search through the PLSDB web interface. Plasmids containing homologous proteins with a minimum query coverage of 40% per high-scoring pair (HSP) were retained. Following manual curation, consolidation of hits from the different query sequences, and removal of redundant entries, a final dataset comprising 447 Evangelion-positive plasmids was used for downstream analyses. Complete plasmid metadata are provided in Supplementary Table S2, whereas representative loci are summarized in Supplementary Table S1.

Taxonomic assignment and plasmid metadata

Host taxonomy, plasmid size, accession numbers and associated metadata were retrieved directly from PLSDB. Plasmids were grouped according to bacterial genus and species to examine the taxonomic distribution of Evangelion homologues and to compare plasmid characteristics across bacterial hosts.

Detection of antimicrobial resistance genes

Antimicrobial resistance genes were identified using ABRicate v1.4.0, screening plasmid sequences against the CARD (Alcock et al., 2023), NCBI AMRFinderPlus (Feldgarden et al., 2021) and ResFinder (Bortolaia et al., 2020) databases using minimum thresholds of 80% nucleotide identity and 70% sequence coverage. Identified genes were manually grouped into functional resistance classes, including β-lactam, aminoglycoside, macrolide, tetracycline, trimethoprim, nucleoside antibiotic, streptothricin, arsenic, biocide and cadmium resistance. Of the 447 Eva01-positive plasmids, 327 encoded at least one antimicrobial resistance determinant.

Plasmid mobility analysis

Plasmid mobility annotations were initially retrieved from PLSDB and supplemented, where required, using MOB-typer (MOB-suite v3.1.9) (Robertson and Nash, 2018). Plasmids were classified as conjugative, mobilisable, oriT-bearing or non-mobilisable based on predicted relaxases, mating-pair formation systems and origins of transfer. Relaxase families and oriT classifications were incorporated into the final plasmid metadata used for downstream visualization.

Comparative plasmid genomic analysis

Representative Eva01-containing plasmids were selected to illustrate the major genomic organizations identified across the dataset while minimizing redundancy among closely related plasmids. Conserved gene neighbourhoods were compared using clinker (Gilchrist and Chooi, 2021) and visualized as interactive gene-cluster alignments in a web browser. Homologous proteins were linked according to amino acid sequence similarity, and genes were manually annotated according to predicted functions, including antimicrobial resistance determinants, plasmid mobility genes and accessory proteins. Representative loci were manually curated for mobility genes, IS elements, integrases, recombinases, defence systems and phage structural genes (Supplementary Table S1).

Defence-system and genomic-context annotation

Representative Evangelion-containing loci were analysed for known and putative defence systems using PADLOC (Payne et al., 2022) and DefenseFinder (Mordret et al., 2026). For Eva01, Eva02 and Eva03 loci, genomic-context analyses were additionally performed using Hoodini, which integrates defence-system prediction and mobile-genetic-element annotation workflows, including PADLOC, DefenseFinder, geNomad and protein-domain searches. Hoodini analyses were performed using COG domain annotation and enabled detection of protein links and additional genomic-context features. Results were manually curated and integrated with independent sequence- and structure-based analyses. Representative annotations are summarized in Supplementary Table S1 and genomic-context analyses are shown in Figure S4.

Phage escaper isolation

Spontaneous escaper mutants were isolated by challenging *S. aureus* strains expressing Eva01 with bacteriophages ϕMR003 or ϕ74. To facilitate the recovery of escaper phages while maintaining selective pressure, bacterial cultures were prepared as a 1:1 mixture of cells carrying pEva01v3 and cells harbouring the empty vector pAH0746. Following overnight infection, lysates were sterilized using 0.2 µm syringe filters (Minisart®, Sartorius Stedim Biotech) to remove bacterial cells.

Individual plaques capable of forming on Eva01-expressing bacterial lawns were picked, purified through repeated plaque isolation, and propagated on Eva01-containing strains. Escape phenotypes were confirmed by determining the efficiency of plating and spot assay profiles on both Eva01-expressing and empty-vector control strains. Escaper phages exhibiting little or no reduction in infectivity relative to the control strain were retained for downstream phenotypic characterization and whole-genome sequencing.

Oxford Nanopore sequencing of single phage plaques

Individual candidate escaper plaques were first confirmed by spot assay on susceptible bacterial lawns. Agar plugs were collected from the centre of individual plaques using sterile 1 mL pipette tips and transferred into 100 µL SM buffer. Samples were vortexed and incubated for 1 h at room temperature to allow phage particles to diffuse from the agar. Agar debris was removed by centrifugation at 13,000 × g for 5 min, and 10 µL of the resulting supernatant was transferred to a 96-well plate.

Samples were treated with 0.01 U DNase I (Thermo Fisher Scientific) for 60 min at 37°C to remove contaminating bacterial DNA, followed by heat inactivation at 95°C for 10 min, which simultaneously released encapsidated phage DNA. Whole-genome amplification was performed using the EquiPhi29 DNA Amplification Kit (Thermo Fisher Scientific) with proportionally scaled reaction volumes. Amplified DNA was subsequently debranched using 10 U S1 nuclease (Thermo Fisher Scientific) at 25°C for 30 min, followed by enzyme inactivation at 95°C for 10 min. DNA concentrations were determined using the Qubit dsDNA Broad Range Assay Kit (Thermo Fisher Scientific).

Sequencing libraries were prepared using the Rapid Barcoding Kit (SQK-RBK114.24 or SQK-RBK114.96; Oxford Nanopore Technologies) and sequenced on a GridION instrument equipped with R10.4.1 flow cells. Reads were basecalled using Dorado v0.9.0 in high-accuracy mode before adapter trimming. Genome assemblies were generated using Flye v2.9.5 (Kolmogorov et al., 2019) and polished by two rounds of Medaka v2.0.0. Genome completeness was evaluated using CheckV v1.0.3 (Nayfach et al., 2021),

taxonomy was assigned using TaxMyPhage v0.3.3 (Millard et al., 2025), and genomes were annotated using Pharokka v1.7.5 (Bouras et al., 2023) with the PHROGS database.

Illumina sequencing of phage escaper mutants

Phage DNA extraction

Phage genomic DNA was extracted from 1 mL sterile-filtered phage lysate using the Phage DNA Isolation Kit (Norgen Biotek) following nuclease pretreatment to eliminate contaminating bacterial nucleic acids. Lysates were supplemented with 20 U RNase-free DNase I (Thermo Fisher Scientific), 1 µL RNase A (Omega Bio-tek) and $MgCl_2$ to a final concentration of 10 mM before incubation at 37°C for 30 min. Nuclease activity was terminated by adding EDTA to a final concentration of 20 mM.

Phage particles were lysed by addition of Lysis Buffer B (Norgen Biotek) and Proteinase K (20 mg mL^{-1}; Thermo Fisher Scientific), followed by incubation at 55°C for 60 min and an additional incubation at 65°C for 15 min. DNA purification was performed according to the manufacturer's instructions. DNA was eluted in 50 µL nuclease-free water and quantified using a Qubit 4 fluorometer with the dsDNA High Sensitivity Assay Kit (Thermo Fisher Scientific).

Illumina library preparation and sequencing

Sequencing libraries were prepared using the Nextera XT DNA Library Preparation Kit (Illumina) following the manufacturer's protocol using 1 ng purified phage DNA as input. Libraries were indexed using the Nextera XT Index Kit v2 (Illumina), purified using AMPure XP magnetic beads (Beckman Coulter), quantified using the Qubit dsDNA High Sensitivity Assay Kit, pooled in equimolar amounts and sequenced by Novogene using paired-end Illumina sequencing.

Escaper mutation identification

Illumina reads from escaper mutants were analysed by comparison with the corresponding parental phage genomes. Reads from ϕMR003 escapers were mapped against the complete ϕMR003 reference genome (GenBank accession AP019522), whereas ϕ74 escapers were analysed using the in-house wild-type ϕ74 reference assembly generated in this study.

Sequence variants were identified using breseq v0.40.1 in consensus mode (Deatherage and Barrick, 2014). Candidate mutations, including single-nucleotide substitutions, short insertions or deletions and structural variants, were manually inspected using Geneious Prime v2026.1.2 to confirm read support and genomic context. Structural variants identified within homing endonuclease loci were further evaluated using read-

depth profiles and junction evidence. Escapers available only as complete genome assemblies were additionally compared with the parental reference genome by whole-genome alignment in Geneious Prime to validate structural rearrangements and large deletions. All mutations are summarized in Supplementary Table S6.

Comparative phage genome analysis

Complete genomes of representative staphylococcal bacteriophages were retrieved from the NCBI GenBank database using the accession numbers listed in Supplementary Table S6. The genome sequence of ϕ74 was assembled from Illumina sequencing data generated in this study and used as the reference genome for downstream comparative analyses. To ensure consistent gene prediction and functional annotation across all genomes, both publicly available phage genomes and the ϕ74 assembly were re-annotated using Pharokka v1.7.5 with default parameters and the PHROGS database (Bouras et al., 2023). Comparative genome analyses were performed using the resulting standardized annotations to identify conserved genomic regions, homologous proteins, and candidate escape mutations. Genome visualizations were generated from the uniformly annotated assemblies.

Protein structure prediction and structural analysis

Representative Evangelion proteins, experimentally characterized TIR-domain proteins, and selected homologues were analysed using a combination of experimentally determined structures and computationally predicted models (Supplementary Table S5). Where available, experimentally resolved structures were obtained from the Protein Data Bank (PDB) (Berman et al., 2000), whereas high-confidence predicted models were retrieved from the AlphaFold Protein Structure Database (Varadi et al., 2022). Proteins lacking available structural models were predicted using the AlphaFold3 server (Abramson et al., 2024).

Predicted structures were used for domain annotation, structural comparisons, visualization of conserved residues, and interpretation of mutational analyses. Where indicated, protein-ligand complexes were generated using the ligand prediction framework implemented within AlphaFold3 to examine potential interactions with NAD^+, ADP, ADP-ribose, cyclic ADP-ribose and other candidate ligands. For AlphaFold-generated models, local confidence scores (predicted Local Distance Difference Test; pLDDT) were used to assess the reliability of individual structural regions. Structural interpretations were restricted to regions with moderate to high prediction confidence.

Structural similarity between Evangelion proteins and representative TIR-domain proteins was assessed using the RCSB PDB Pairwise Structure Alignment server employing the TM-align algorithm (Zhang and Skolnick, 2005). Pairwise structural

comparisons were performed using either experimentally determined structures or AlphaFold-predicted models generated in this study or obtained from the AlphaFold Protein Structure Database. Structural superposition, visualization, figure preparation and residue annotation were performed using UCSF ChimeraX v1.11.1 (Pettersen et al., 2021). Representative proteins analysed in this section are listed in Supplementary Table S5.

Multiple sequence alignment

Protein sequences were aligned using MAFFT v7.526 (Katoh and Standley, 2013) with default parameters. Multiple sequence alignments were visualized and prepared for publication using ESPript 3.2 (Robert and Gouet, 2014). Residue conservation was displayed using the BLOSUM62 similarity colouring scheme with a global conservation threshold of 0.7. Alignments were formatted in landscape orientation using an A3 page layout, a font size of 7, 80 residues per line, and without display of the consensus sequence.

Untargeted polar metabolomics

Overnight cultures of *S. aureus* strains carrying plasmids encoding wild-type Eva01 or Eva01 variants were diluted 1:50 into 30 mL fresh TSB supplemented with the appropriate antibiotics and 10 mM $CaCl_2$. Cultures were grown at 37°C with shaking to an OD600 of approximately 0.25. For each condition, 8 mL of culture was infected at a multiplicity of infection (MOI) of 2 with ϕMR003, ϕMR003 escaper, or ϕ74, as indicated. At 15 min post-infection, 6 mL of culture was harvested by centrifugation at 5,000 × g for 2-3 min at 4°C. Cell pellets were washed once with ice-cold 0.9% NaCl, centrifuged again, and quenched by resuspension in 80% methanol/water pre-cooled to -20°C. Samples were stored at -80°C until analysis.

Untargeted polar metabolomics was performed by Cmbio/Clinical Microbiomics. Cell samples were extracted by repeated temperature-shock lysis combined with bead beating. Methanol-quenched samples were transferred to bead-beating tubes containing 0.1 mm ceramic beads and rinsed twice with methanol/water. Samples were bead beaten for four cycles of 30 s at 30 Hz with intermittent cooling at -20°C, followed by three freeze-thaw cycles in liquid nitrogen and thawing on ice. Extracts were centrifuged at 15,000 × g for 5 min at 4°C, dried under nitrogen flow, and reconstituted in acetonitrile/water.

Polar metabolites were analysed by hydrophilic interaction liquid chromatography coupled to high-resolution mass spectrometry (HILIC-HRMS). Reconstituted extracts were filtered and fortified with stable isotope-labelled internal standards before injection. Chromatographic separation was performed on an ACQUITY Premier BEH

Amide column (1.7 µm, 2.1 × 100 mm; Waters) using an Orbitrap Exploris 240 mass spectrometer (Thermo Fisher Scientific) equipped with an electrospray ionisation source. Separation was performed using a 12-min two-step gradient at 450 µL min-1 followed by 4 min re-equilibration. The column temperature was maintained at 30°C and the injection volume was 2 µL. Eluent A consisted of 10 mM ammonium formate in acetonitrile, pH 10, and eluent B consisted of 10 mM ammonium formate in 40% acetonitrile, pH 10, with 0.1% medronic acid. Data were acquired with polarity switching in positive and negative ionisation modes over m/z ranges of 60-200 and 200-900 at a resolution of 60,000. Iterative data-dependent MS/MS acquisition was performed on pooled quality-control samples using TopN acquisition with N = 10 and stepped collision energies of 20, 40 and 60.

Raw LC-MS data were processed using Compound Discoverer 3.4 and Skyline 25.1. Features were detected, aligned, grouped into compound entries, curated to remove low-quality signals and background features, and annotated using accurate mass, retention time and MS/MS information. Metabolite annotations were assigned using four confidence levels, with level 1 corresponding to matches based on accurate mass, MS/MS spectra and retention time from standards analysed on the same system. Libraries searched included the Human Metabolome Database, ChEBI, BioCyc and the *E. coli* Metabolome Database, with a maximum mass deviation of 3 ppm.

Pooled quality-control samples were generated from equal aliquots of all extracts and injected at the beginning, end and regular intervals throughout the analytical sequence. A QC dilution series was included to evaluate detector linearity and matrix effects. Core data were defined as compounds with descriptive power greater than 2.5 and high-confidence annotations. Statistical analyses were performed on transformed data using t-tests with Benjamini-Hochberg correction for multiple testing, with a false-discovery rate threshold of 0.05. Principal component analysis was used to assess sample clustering and analytical reproducibility.

Digital PCR quantification of intracellular phage DNA

Intracellular phage genome accumulation was quantified by digital PCR following infection of *S. aureus* strains carrying either Eva01 or the corresponding empty-vector control. Overnight cultures were diluted 1:50 into fresh TSB containing the appropriate antibiotics and grown to early exponential phase (OD600 ≈ 0.25). Cultures were infected with wild-type ϕMR003 or the escape mutant ϕMR003 E10 at the indicated multiplicity of infection. Samples were collected at 0, 5 and 40 min post-infection.

To terminate phage infection, EDTA was added immediately to each culture to chelate divalent cations required for phage adsorption, and samples were transferred onto ice. Cells were collected by centrifugation and extracellular phage particles were removed by

treatment with DNase I prior to cell lysis, thereby degrading extracellular phage DNA while preserving intracellular bacterial and phage genomes. Following DNase treatment, cells were washed and pelleted before genomic DNA extraction using the GenElute™ Bacterial Genomic DNA Kit (Sigma-Aldrich). Bacterial pellets were pre-treated with lysostaphin (Sigma-Aldrich) to digest the cell wall prior to DNA purification, following the manufacturer's protocol. DNA concentrations were determined using a Qubit 4 fluorometer (Thermo Fisher Scientific), and template input was standardized to approximately 0.2 ng per reaction.

Digital PCR assays targeted two independent ϕMR003 loci representing distinct stages of phage replication. The capsid locus was selected as a marker within the structural region of the phage genome, whereas the *uvs*X recombinase locus represented a replication/recombination-associated region. The chromosomal *gyr*B gene served as an internal reference for normalization of DNA recovery and template input. Primer sequences are provided in Supplementary Table S4.

Digital PCR reactions were performed using the QIAcuity Nanoplate 8.5K platform (QIAGEN) with EvaGreen chemistry according to the manufacturer's recommendations. Reactions contained QIAcuity EvaGreen Master Mix, target-specific primer pairs, and approximately 0.2 ng genomic DNA. Absolute target copy numbers were calculated using QIAcuity Software and expressed as copies per microlitre of reaction mixture.

Phage DNA abundance was normalized to chromosomal gyrB copy number and expressed as target/gyrB ratios. Normalized values were log2-transformed before statistical analysis and visualization. Reactions containing fewer than 4,000 accepted partitions or fewer than 10 positive partitions were excluded from quantitative analyses. Saturated reactions were retained for graphical representation but excluded from statistical comparisons. Biological replicates from independent infection experiments were combined following quality-control filtering.

Protein expression and purification

The Eva01 coding sequence was cloned into the pET-28a(+) expression vector (Novagen), resulting in an N-terminal histidine (His_6)-tagged construct. The N-terminal His tag was retained throughout purification and was not removed. Recombinant plasmids were transformed into *E. coli* BL21(DE3) cells for protein expression.

Protein expression was performed using Overnight Express™ Instant TB Medium (Novagen, Cat. No. 71491-5CN) according to the manufacturer's instructions. Cultures were incubated overnight at 18°C with shaking to promote soluble protein expression. Cells were harvested by centrifugation and resuspended in lysis buffer containing 20 mM Tris-HCl (pH 7.5) and 250 mM NaCl before disruption by sonication. Cell lysates were

clarified by centrifugation and recombinant Eva01 was purified by immobilized metal affinity chromatography using TALON Metal Affinity Resin (Takara Bio, Japan) according to the manufacturer's recommendations.

Purified protein was concentrated and exchanged into storage buffer (20 mM Tris-HCl, pH 7.5, 150 mM NaCl, 5% (v/v) glycerol) using Amicon Ultra centrifugal filter units (10 kDa molecular-weight cutoff; Merck, Cat. No. UFC9010). Protein aliquots were stored at -80°C until use. Protein purity was assessed by SDS-PAGE.

Mass photometry

Mass photometry measurements were performed using a TwoMP mass photometer (Refeyn Ltd., Oxford, United Kingdom). Purified Eva01 protein was diluted in phosphate-buffered saline (PBS), and 10 µL of sample was added to the measurement chamber immediately before data acquisition. Measurements were performed according to the manufacturer's instructions. Data were analysed using DiscoverMP software (Refeyn Ltd.) to determine the molecular mass distribution and estimate the oligomeric state of Eva01.

Electrophoretic mobility shift assays

DNA-binding activity of Eva01 was evaluated using electrophoretic mobility shift assays (EMSAs). DNA substrates representing blunt-ended double-stranded DNA, single-stranded DNA, 3' overhang substrates, bubble DNA and gapped DNA were generated by annealing synthetic oligonucleotides (Eurofins Genomics). DNA oligonucleotide sequences used for EMSA are listed in Supplementary Table S4.

Approximately 15 nM DNA substrate was incubated with 16 nM purified Eva01 in 50 µL NEBuffer 2 (New England Biolabs) for 40 min at 30°C. For concentration-dependent binding assays, Eva01 concentrations of 4, 8, 16 and 32 nM were used.

Reaction mixtures were combined with native loading dye and resolved on 4-16% NativePAGE Bis-Tris gels (Invitrogen) under non-denaturing conditions at 4°C for 80 min. Gels were stained using SYBR Gold (Invitrogen) and imaged using a gel documentation system.

Sequence clustering and similarity network analysis

DUF4062-containing proteins were identified from the InterPro database (Paysan-Lafosse et al., 2024) by querying the Pfam DUF4062 family (PF13271) (Mistry et al., 2021). All associated UniProt entries (The UniProt Consortium, 2025) were retrieved and filtered to retain bacterial proteins suitable for downstream analyses.

To visualize the overall sequence diversity of the DUF4062 family, all bacterial DUF4062-containing proteins were subjected to all-against-all BLAST P-values in a force-directed layout using CLANS (Frickey and Lupas, 2004). Pairwise similarities were calculated using the default CLANS settings, and clusters were visualized after convergence. Representative Evangelion lineages identified from the maximum-likelihood phylogeny were mapped onto the resulting similarity network to facilitate interpretation of the major DUF4062 families.

To reduce redundancy for phylogenetic reconstruction, protein sequences were clustered using MMseqs2 v18.8cc5c (Steinegger and Söding, 2017) at 40% amino acid identity and 60% alignment coverage, yielding representative sequence clusters. Experimentally characterized Evangelion homologues and selected reference proteins were subsequently added to generate the final phylogenetic dataset.

Phylogenetic reconstruction

Protein sequences were aligned using MAFFT v7.526 (Katoh and Standley, 2013) with the L-INS-i algorithm. Alignment columns containing less than 20% occupancy were removed prior to tree reconstruction. Maximum-likelihood phylogenies were inferred using IQ-TREE v3.1.1 (Minh et al., 2025) with automatic model selection using ModelFinder (Kalyaanamoorthy et al., 2017). Branch support was estimated using 1,000 ultrafast bootstrap replicates (UFBoot2) (Hoang et al., 2018). Trees were visualized and annotated using Interactive Tree Of Life (iTOL) v7.6 (Letunic and Bork, 2024). For the DUF4062/TIR-domain core phylogeny shown in Figure 6A-B, IQ-TREE selected the Q.YEAST+G4 substitution model according to the Bayesian Information Criterion.

Genomic context analysis of Evangelion loci

Genomic regions containing representative DUF4062 homologues were retrieved from their corresponding sequence records. Protein-coding genes were predicted using Prokka v1.15.6 in metagenome mode with insertion-sequence annotation enabled (Seemann, 2014).

Representative DUF4062 proteins were mapped back to their corresponding coding sequences using DIAMOND v2.1.25 (Buchfink et al., 2021) with an E-value threshold of 1×10^{-20}, minimum amino acid identity of 70%, and minimum query coverage of 70%. The resulting annotations were used to define the local genomic environment surrounding each Evangelion homologue**.**

Classification of mobile genetic element contexts

Genomic contexts were classified using geNomad v1.12.0 (Camargo et al., 2023) to identify plasmid- and prophage-associated regions. Functional annotations generated by Prokka were further screened using curated keyword searches to identify genes

associated with conjugation, recombination, transposition and bacterial defence systems.

Each Evangelion locus was classified hierarchically as plasmid-associated, prophage-associated, integrative conjugative element (ICE)-associated, defence-associated chromosomal, or unresolved chromosomal according to geNomad predictions together with the presence of mobility- or defence-associated genes within a 50-kb genomic window. Transposases and insertion-sequence elements were recorded independently of the primary genomic-context classification.

Tree visualization

Host taxonomy, genomic-context classifications and neighbouring mobility-associated genes were imported to Interactive Tree of Life (iTOL) v7.6 (Letunic and Bork, 2024) for visualization of the phylogeny. Experimentally characterized Evangelion homologues were highlighted as reference sequences, and final figures were generated using iTOL.

Statistical analysis and visualization

Statistical analyses were performed in GraphPad Prism 10 unless otherwise indicated. The statistical tests, sample sizes (n), and definitions of error bars are provided in the corresponding figure legends. Differences were considered statistically significant at $P < 0.05$. Data visualization was performed using Matplotlib and Seaborn. Distribution analyses were visualized using violin plots with embedded boxplots. ARG class combinations were represented using UpSet-style plots, and plasmid mobility categories were visualized using donut charts and horizontal bar plots. Figures were exported in PNG and SVG formats.

Data and code availability

Sequencing data generated in this study will be deposited in the NCBI Sequence Read Archive (SRA) prior to publication. Genome assemblies will be deposited in GenBank. Untargeted metabolomics datasets will be deposited in an appropriate public metabolomics repository. Custom scripts used for bioinformatic analyses and data processing will be made available through GitHub upon publication.

Supplementary Figure legends

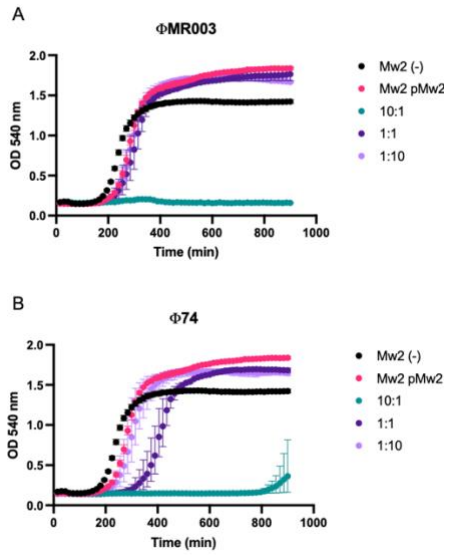


Figure S1. pMw2 protects *S. aureus* against *Silviavirus* infection across a range of phage burdens. Related to Figure 1. (A) Growth curves (*n*=3) of *S. aureus* Mw2 carrying pMw2 or a plasmid-cured derivative following infection with ϕMR003 at different multiplicities of infection (MOI). (B) Growth curves (*n*=3) following infection with ϕ74 at different MOIs.

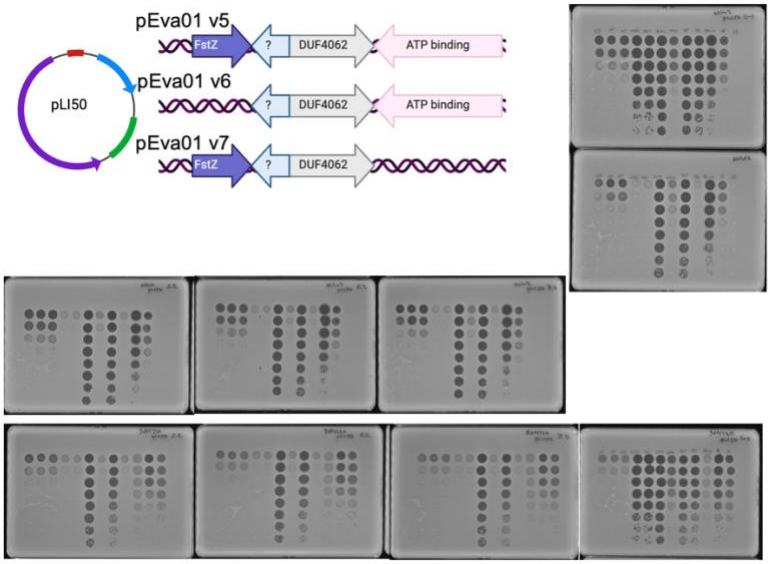


Figure S2. Definition of the minimal functional Eva01 locus and complementation of defence phenotype in Mw2. Related to Figure 1. Representative spot assays of additional Eva01 constructs containing different combinations of upstream and downstream regions surrounding the DUF4062-containing gene. Constructs retaining the DUF4062 core and associated regulatory sequences confer protection against ϕMR003, whereas constructs lacking essential regions fail to protect against phage infection.

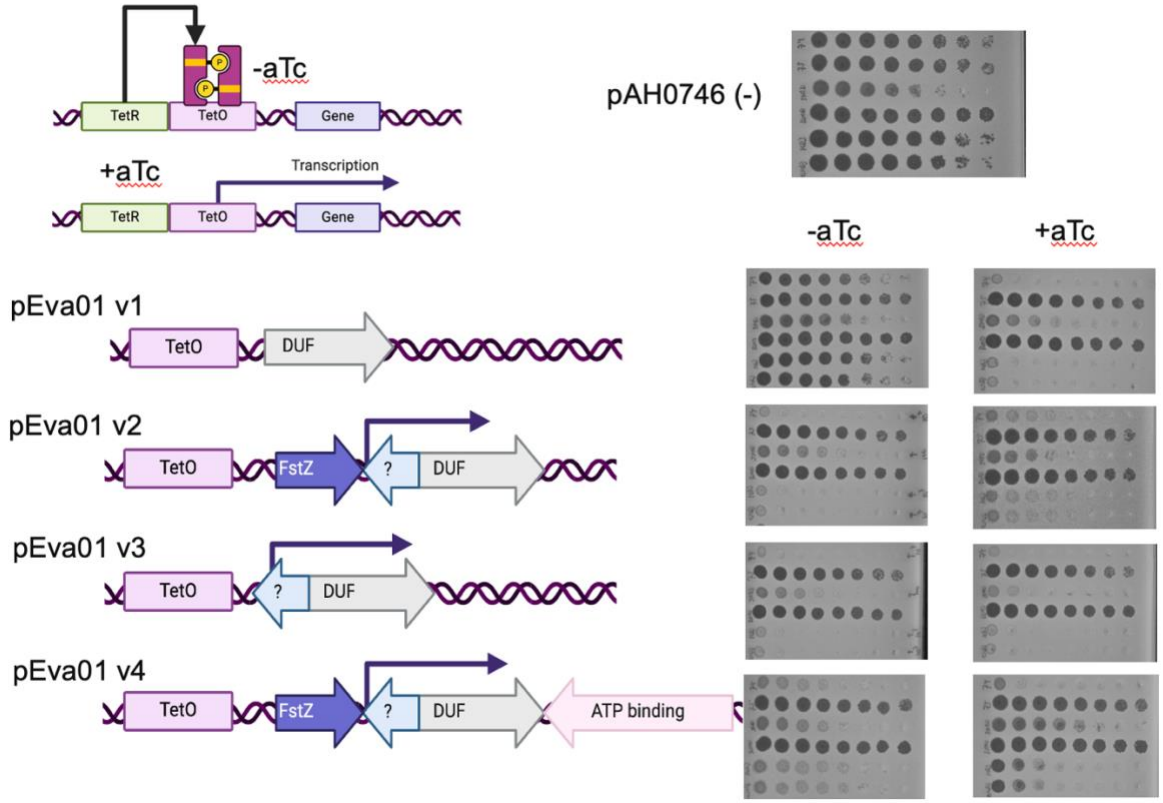


Figure S3. Inducible expression and functional mapping of Eva01. Related to Figure 1. Schematic of the tetracycline-inducible expression system used to define the minimal Eva01 locus. Representative spot assays performed in the presence and absence of anhydrotetracycline (aTc) demonstrate defence activity of constructs pEva01v1-v4. Protection is retained in constructs containing the minimal Eva01 region, consistent with basal expression from local regulatory elements.

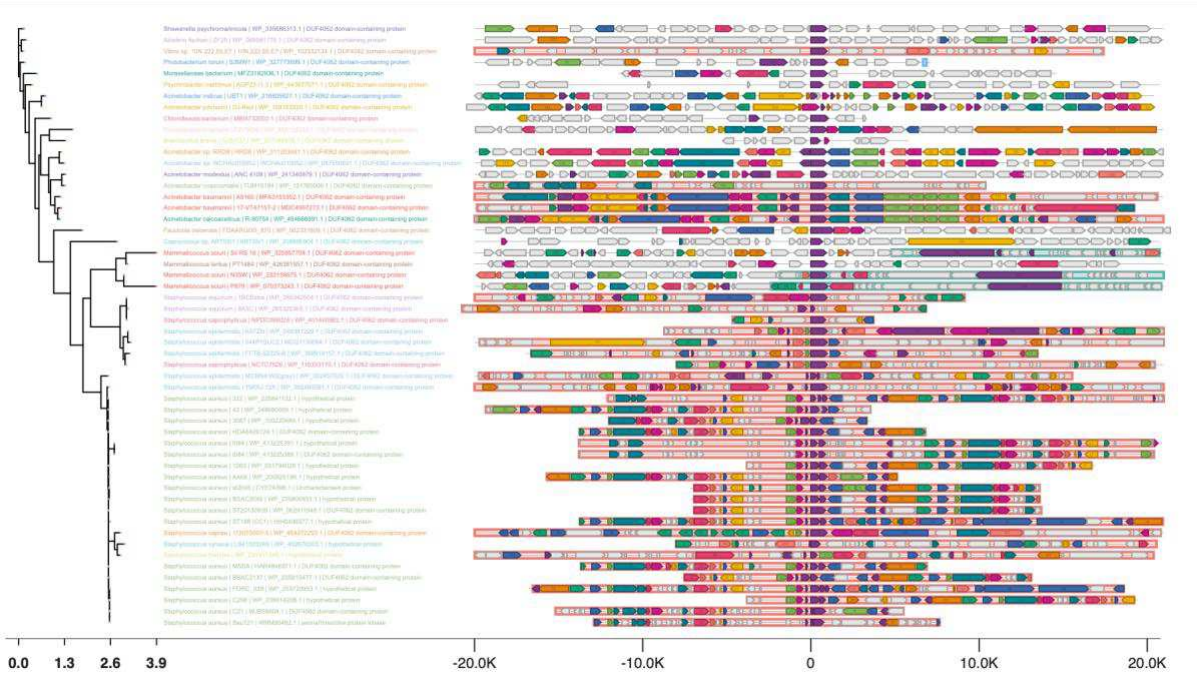


Figure S4. Comparative genomic context of Eva01-containing plasmids. Related to Figure 1. Phylogenetic relationships and gene neighbourhoods of representative Eva01-positive plasmids identified from public databases. Conserved Eva01 loci are positioned adjacent to diverse combinations of antimicrobial-resistance genes, mobility-associated genes, toxin-antitoxin modules and hypothetical proteins, illustrating the diversity of Eva01-containing plasmid backbones.

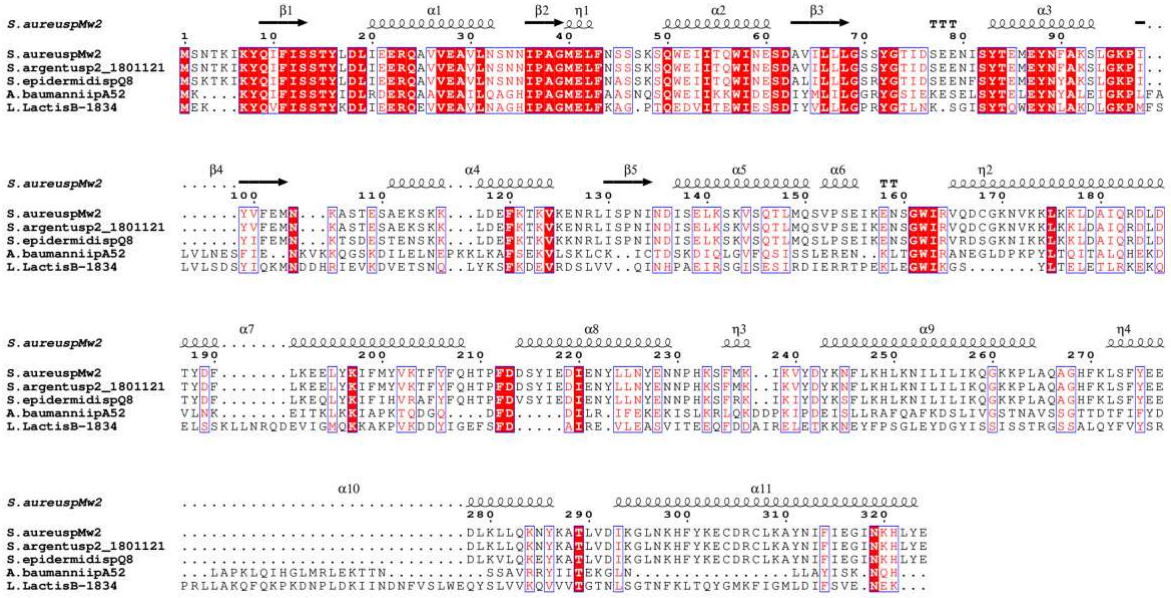


Figure S5. Conservation of DUF4062 motifs across Evangelion proteins. Related to Figure 3. Multiple sequence alignments of representative Evangelion proteins from diverse bacterial hosts. Conserved residues and secondary-structure elements are indicated. The aromatic core motif, acidic-SYT region and DUF4062-specific Q/W/E motif are strongly conserved across the family. Residues selected for mutagenesis are highlighted.

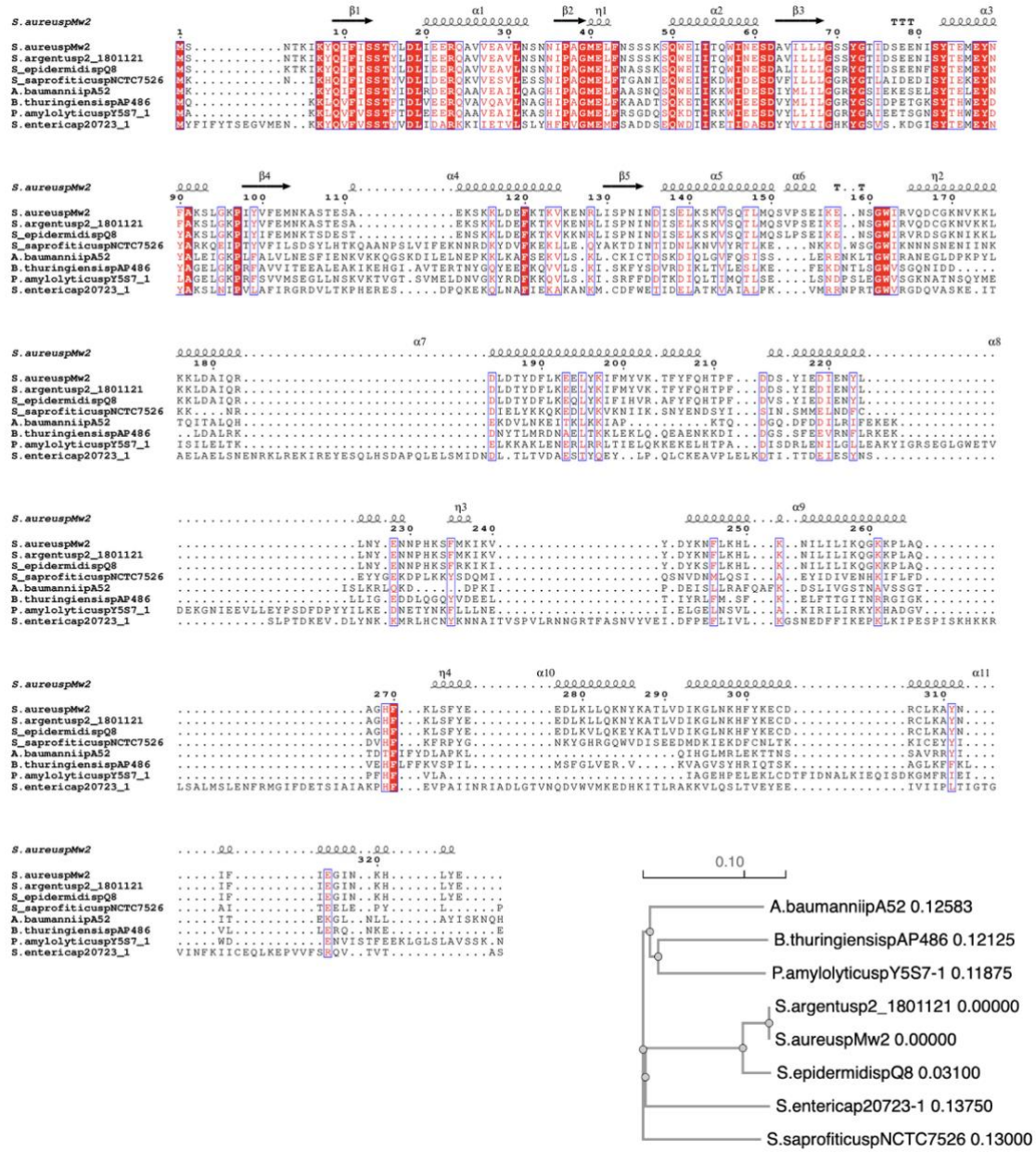


Figure S6. Conservation of Evangelion-associated DUF4062 proteins. Related to Figure 3. Expanded sequence alignments and phylogenetic analysis of representative Evangelion homologues. Conserved DUF4062 residues remain identifiable despite extensive divergence in surrounding regions. The accompanying phylogeny illustrates the evolutionary relationships among representative homologues used throughout this study.

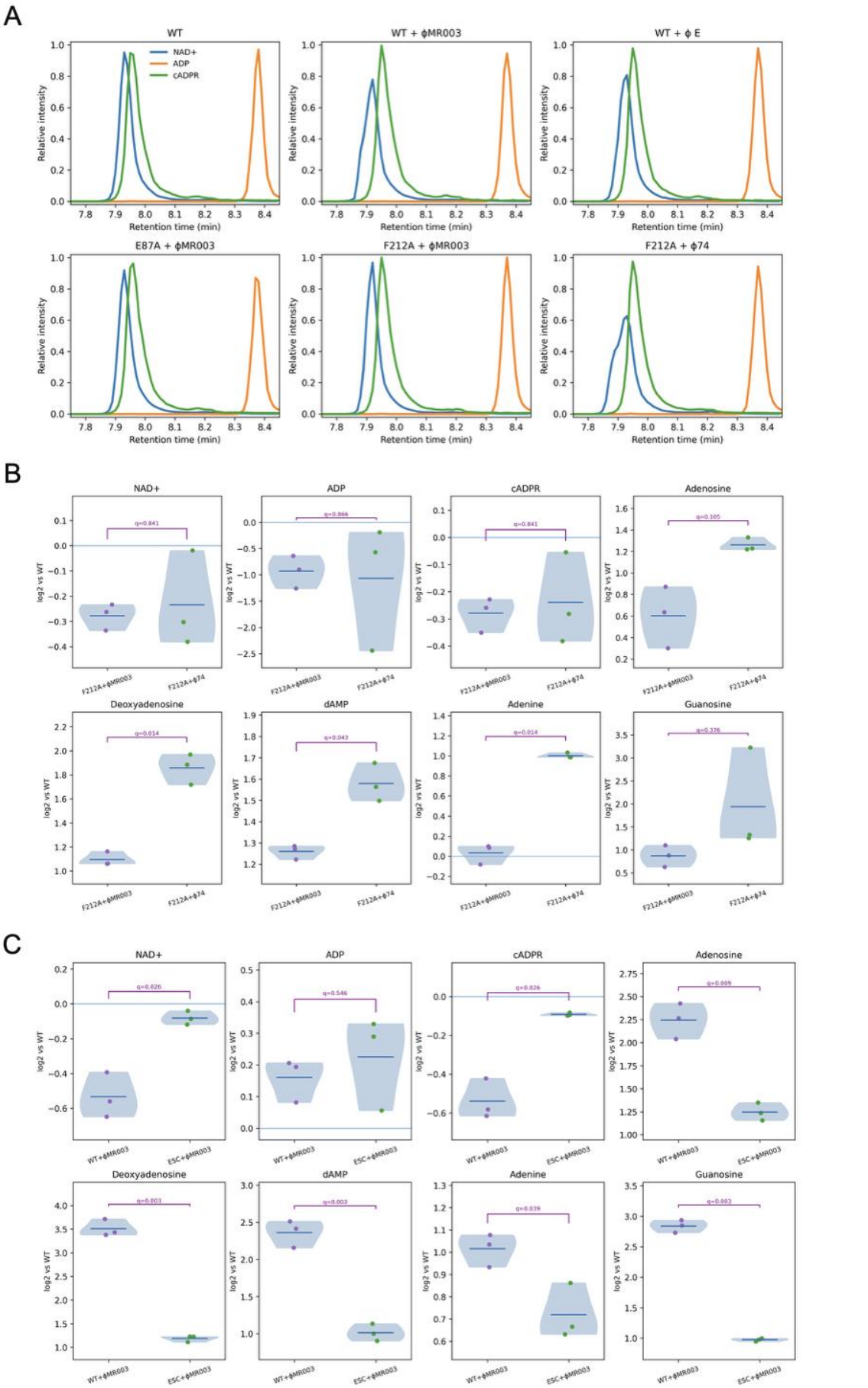

A
WT
WT + ϕMR003
WT + ϕ E
E87A + ϕMR003
F212A + ϕMR003
F212A + ϕ74
NAD+
ADP
cADPR
Relative intensity
Retention time (min)
B
NAD+
ADP
cADPR
Adenosine
Deoxyadenosine
dAMP
Adenine
Guanosine
log2 vs WT
F212A+ϕMR003
F212A+ϕ74
C
NAD+
ADP
cADPR
Adenosine
Deoxyadenosine
dAMP
Adenine
Guanosine
log2 vs WT
WT+ϕMR003
ESC+ϕMR003

Figure S7. Additional metabolomic and structural analyses of Eva01. Related to Figure 4. (A) Representative chromatograms showing metabolite profiles in strains expressing wild-type or mutant Eva01 variants before and after ϕMR003 infection. (B-C) Quantification of additional nucleotide-associated metabolites altered during Evangelion activation. These data support widespread remodelling of nucleotide metabolism during Eva01-mediated defence.

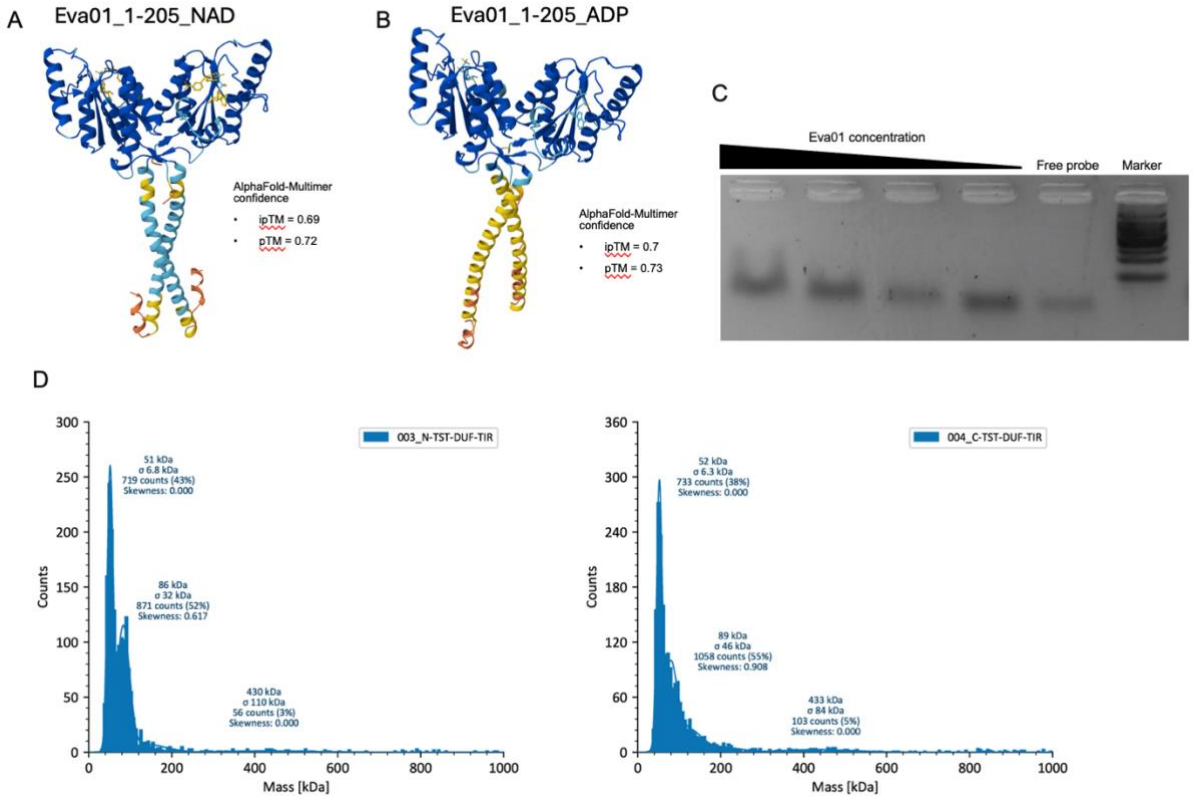


Figure S8. Predicted oligomeric assemblies, DNA binding, and mass photometry analysis of Eva01. Related to Figure 4. (A-B) AlphaFold3 models of Eva01 DUF4062-containing regions in the presence of NAD^+ or ADP. Predicted oligomeric assemblies display stacked interfaces involving conserved DUF4062 regions. (C) Concentration-dependent binding of Eva01 to the 3' overhang DNA substrate. Approximately 15 nM DNA was incubated with increasing concentrations of purified Eva01 (4, 8, 16 and 32 nM) before separation by native PAGE. Progressive DNA mobility shifts were observed with increasing Eva01 concentration. (D) Mass photometry reveals multiple species with masses compatible with monomeric, dimeric and higher-order assemblies, supporting the ability of Eva01 to self-associate in solution.

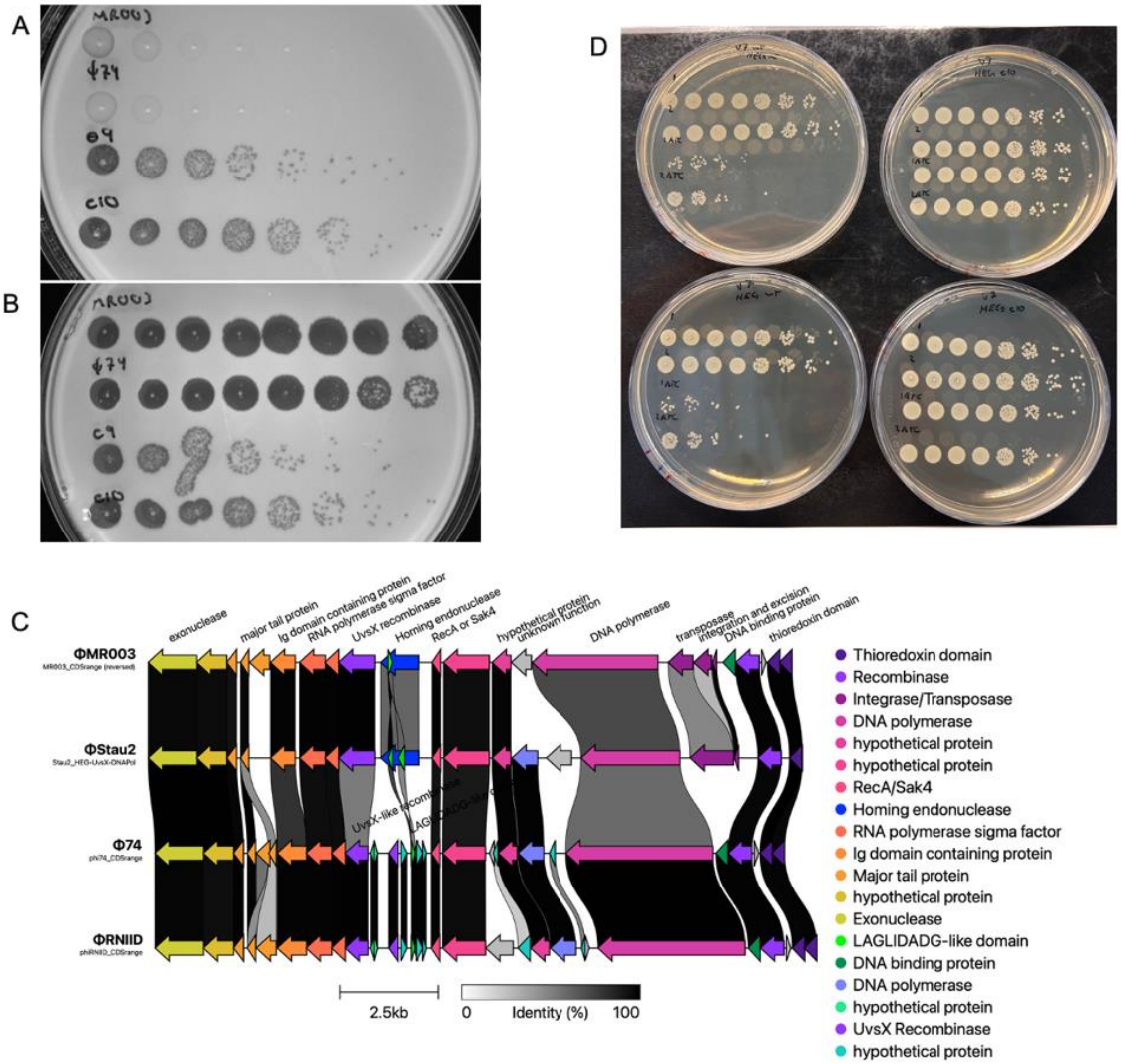


Figure S9. Additional characterization of phage escapers and replication-associated loci. Related to Figure 5. (A-B) Representative spot assays showing infection of Eva01-expressing strains by independent ϕMR003 and ϕ74 escaper mutants. (C) Comparative genomic analysis of additional *Silviavirus* genomes demonstrating conservation of the replication-associated locus targeted by escaper mutations. (D) Representative plating assays illustrating differential susceptibility of wild-type and mutant phages.

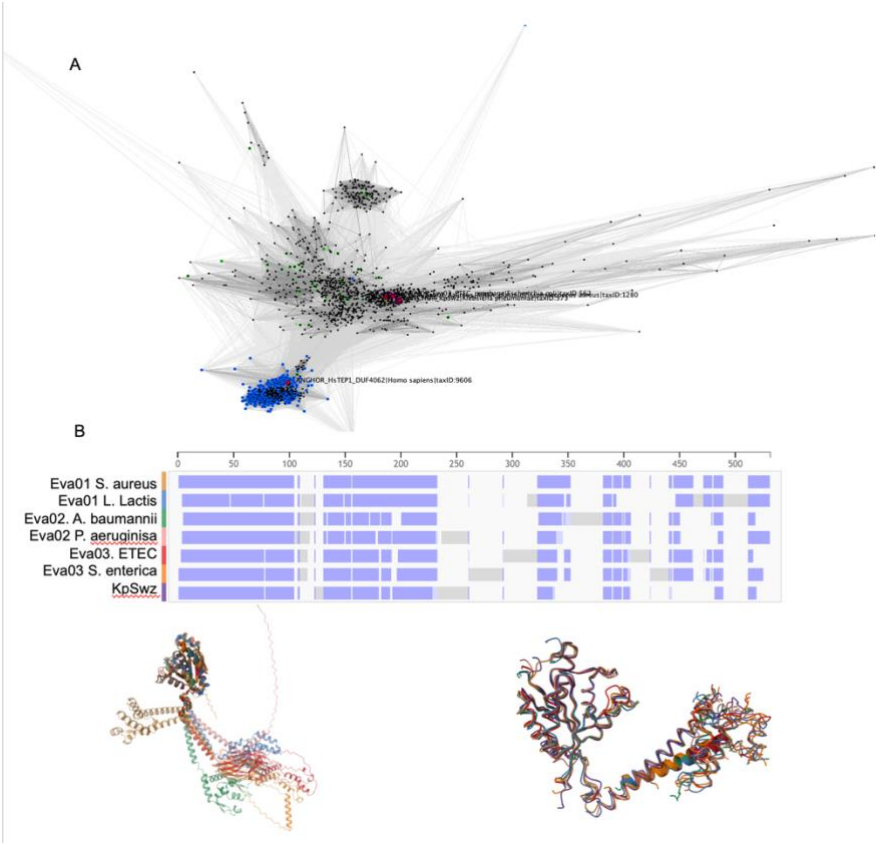


Figure S10. Expanded evolutionary analysis of DUF4062-containing defence systems. Related to Figure 6. (A) Sequence-similarity network of representative DUF4062-containing proteins showing clustering of Evangelion lineages, Swarożyc and TEP1-like proteins. (B) Domain-architecture comparison and structural overlays of representative DUF4062 proteins. Conserved DUF4062 cores are retained despite extensive diversification of auxiliary domains and overall protein architecture.

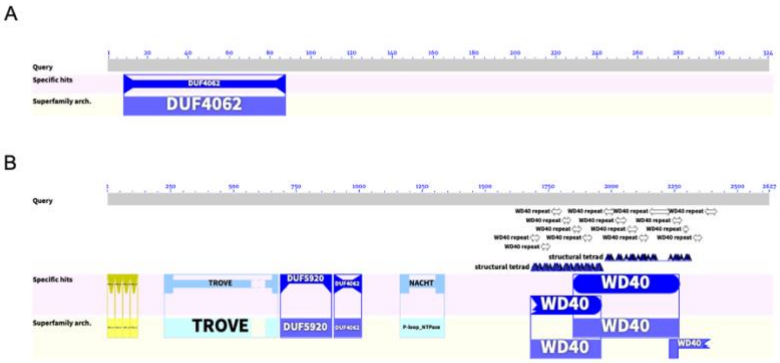
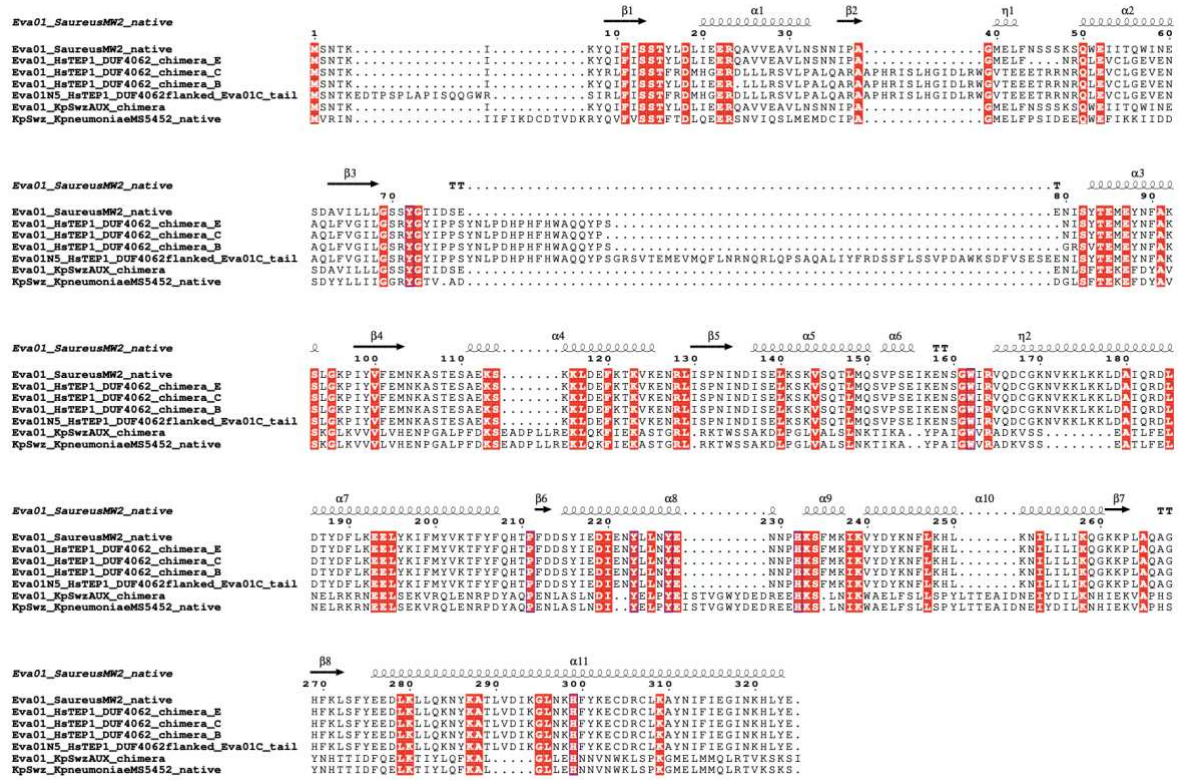


Figure S11. Conserved-domain relationships between Eva01 and TEP1-like proteins. Related to Figure 6 and Figure 7. Conserved-domain searches identifying DUF4062 as the shared feature between Eva01 and bacterial/eukaryotic TEP1-like proteins. Additional domains present in TEP1-like proteins, including TROVE, NACHT and WD40-repeat regions, are indicated.



1419

1420 Figure S12. Structural conservation of DUF4062 regions from Evangelion and TEP1
1421 proteins. Related to Figure 7. Multiple sequence alignment and secondary-structure
1422 comparison of DUF4062-containing regions from Evangelion proteins, TEP1-like proteins
1423 and representative homologues. Conserved residues associated with the predicted
1424 DUF4062 fold are highlighted, supporting an evolutionary relationship between bacterial
1425 Evangelion systems and eukaryotic TEP1-like proteins.

1426

Supplementary Files

This is a list of supplementary files associated with this preprint. Click to download.

- SupplementaryTables.xlsx